Hindawi Publishing Corporation
Shock and Vibration
Volume 2015, Article ID 857978, 23 pages
http://dx.doi.org/10.1155/2015/857978

*Research Article*

# An Experimental Study on Dynamics of a Novel Dual-Belt Continuous Variable Transmission Based on a Newly Developed Test Rig

**Pak Kin Wong, Zhengchao Xie, and Yueqiao Chen**

*Department of Electromechanical Engineering, University of Macau, Taipa, Macau*

Correspondence should be addressed to Zhengchao Xie; zxie@umac.mo

Received 9 March 2015; Revised 11 May 2015; Accepted 18 May 2015

Academic Editor: Roger Serra



A novel dual-belt Van Doorne's continuous variable transmission (DBVCVT) system, which is applicable to heavy-duty vehicles, has been previously proposed by the authors in order to improve the low torque capacity of traditional single-belt CVT. This DBVCVT is a novel design among continuously variable transmissions and is necessary to be prototyped for experimental study, and the analytical dynamic model for this DBVCVT also needs to be experimentally validated. So, this work originally fabricated a prototype of DBVCVT and integrates this prototype to a light-load hardware-in-the-loop test rig by replacing the engine and load equipment with the AC motor and magnetic powder dynamometer. Moreover, with the use of this newly developed test rig, this work implements the experimental study of this DBVCVT for the first time. The comparison of experimental and simulation results validates the previously proposed analytical model for DBVCVT, and some basic characteristics of the DBVCVT in terms of the reliability, speed ratio, and transmission efficiency are also experimentally studied. In all, this developed test rig with the analytical model lays the foundation for further study on this novel DBVCVT.

## 1. Introduction

Continuous variable transmission (CVT) is a type of automatic transmission which is increasingly used in automotive applications. Apart from automatic transmissions, the CVT is also increasingly used in operation of kinetic energy recovery systems and hybrid vehicle operation [1–5]. In fact, the CVT is an ideal design and has many advantages over the other transmissions, such as infinite gear ratios, smoother change of speed ratio, simpler mechanism, and lighter weight. Typically, Van Doorne's CVT based on the single metal pushing V-belt is currently the most popular type of CVT due to its good reliability, durability, and efficiency [6–10]. In view of its popularity, this research focuses on Van Doorne's CVT. Figure 1 shows the model of Van Doorne's CVT and metal pushing V-belt. Despite these advantages, Van Doorne's CVT still has rather large potential for improvement in transmission efficiency. The main reason for inadequate transmission efficiency of modern Van Doorne's CVT is the excessive clamping force in the variator to prevent the metal belt from slip. Higher clamping force results in additional friction losses in the system because of extra mechanical load applying to all variator parts. Excessive clamping force also reduces the life of the steel element because the extrusion force in the element is larger than the barely needed force for transmission of engine power. Moreover, the contact pressure between the V-belt and the pulleys is higher than the minimum required pressure that further increases the wear. So, at the risk of slip, many researches focused on reducing the clamping force in order to increase the transmission efficiency [9, 11].

Similarly, the torque capacity is also one of the main limitations of modern CVTs, which is currently limited by the strength of the steel belt and by the ability to withstand friction wear between torque source and transmission medium [12, 13]. At present, a single-belt Van Doorne's CVT has been developed for the class of 3500 cc vehicles, such as Nissan Maxima, which can handle about 350 N·m torque at 4400 RPM; this is the maximum torque capacity of Van

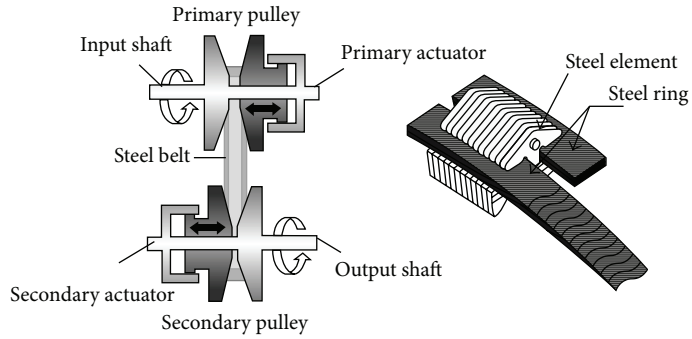


Figure 1: Model of Van Doorne's CVT and metal pushing V-belt [28].

Doorne's CVT so far [14]. In a nutshell, Van Doorne's CVT is currently only applicable to low-torque passenger cars because of limited torque capacity.

Among all the existing researches on CVT systems, very few of them focus on torque capacity enhancement for Van Doorne's CVT; most of existing literature studied the influence of friction characteristic between the belt and the pulley upon the torque capacity in both steady and transient states [15–22].

For large power and torque transmission with the traditional pulley and belt drive system, a dual-belt or multiple-belt system will normally be used instead of a single-belt system. In 2009, the authors showed that the use of dual-rubber belt can improve the torque capacity on a centrifugal-type CVT for the scooter [23]. Therefore, it is of great interest to extend this concept to Van Doorne's CVT system. In the existing literature, there is no dual-belt Van Doorne's CVT available, but Efficient Drivetrains, Inc. developed a similar CVT prototype as shown in Figure 2, which are targeted at both light- and medium-duty applications for either front or rear wheel drive and can support higher torque ranges and greater levels of efficiency than any other CVT transmissions available in the market today [21]. This CVT is also called inline chain CVT and its detailed design was given in [24]. The inline CVT is actually a single chain CVT system, but it connects two single chains in series. Figure 2 shows the series configuration of the two chains that transmits the torque from the first chain to the second chain. Compared to a regular CVT with the same ratio range $i$, the ratio of the first CVT is multiplied by the ratio of the second CVT to achieve the same ratio of a regular CVT; therefore, the two stages of inline CVT have a much smaller individual ratio span. As a result, this inline CVT can be operated closer to around $i = 1$, which can increase the efficiency [25]. However, this inline CVT also has some disadvantages: (1) The inline CVT is slightly larger in the vertical direction: once it is used in heavy-duty vehicles, there must be a very large ground clearance [25]; (2) it needs two separated speed ratio control systems to control the speed ratios of the two sets of pulley and chain drives, resulting in high cost and complexity; (3) it is actually a two-stage single-belt/chain CVT system: the limitation of torque capacity of traditional single-belt/chain CVT systems still exists; (4) as it inherits from the properties of single-belt/chain CVT systems, one of two CVTs still needs to be overclamped; the high clamping force can reduce the transmission efficiency and the life of the component. Besides that, it is very necessary to mention that this inline CVT design uses two chains instead of belts. Different from Van Doorne's CVT with the belt, the disadvantages of the chain are as follows. (1) Chains produce more noise and vibration than Van Doorne's metal pushing V-belts. This is caused by the relatively small number of pins that continuously run into the pulley. (2) A more complicated structure of the chain means the expensive maintenance and repair kits. (3) It is high in cost. (4) The number of pins is effectively halved, lowering the chain stiffness and the strength [26, 27].

To overcome the aforementioned limitations of current single-belt Van Doorne's CVT and the inline CVT, this paper proposes a novel parallel continuously variable transmission. The transmission is named dual-belt Van Doorne's continuously variable transmission (DBVCVT), which can be implemented on heavy-duty vehicles and has significant improvement in torque capacity and efficiency. With the parallel configuration of dual belts, the ratio spans of two belt and pulley sets are the same so that only one speed ratio controller is required as compared with the inline CVT. Moreover, the torque capacities of two identical single-belt CVTs can be added up. Also, the clamping force can be shared with two belts so as to increase the durability of the belts. Even though the authors previously proposed the idea of dual-belt CVT in [29], the design and model at that time were simple and out of the consideration of asynchronous belt motion and so on. Moreover, there was no substantial experimental study in the previous work.

For automatic transmissions, since the transmission mechanism is very complex and difficult for developing an exact analytical model, the hardware-in-the-loop technology as an effective tool has always been widely used to analyze the transmission performance of the automatic transmissions. There are some works considered low-cost hardware-in-the-loop simulation structures in which usually a real transmission control unit (TCU) is connected with a virtual controlled object, adopting a real-time hardware platform to simulate the external environment of the TCU, such as sensor signal and communication interface [30–32]. Hagiwara et al. considered the transmission nonlinearity of the CVT and then built a real-time simulation model of the speed ratio change to verify the TCU speed ratio control algorithm.

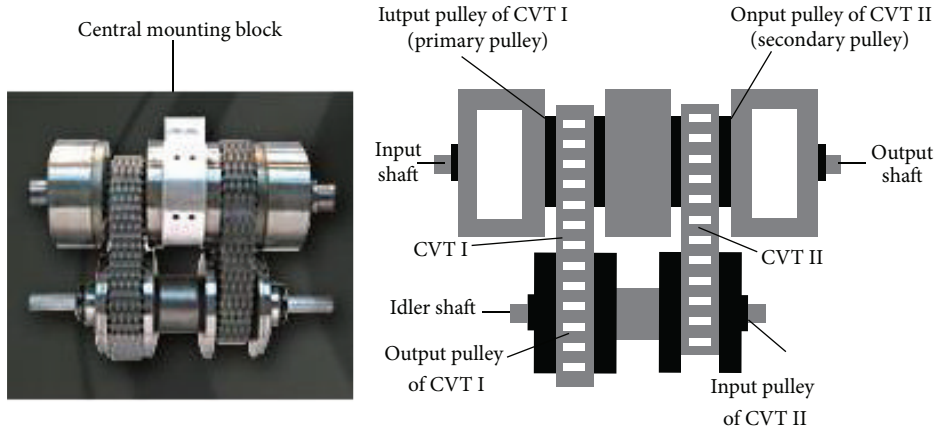


Figure 2: Inline chain CVT [21].

Bai et al. used the SimDriveline Simulink toolbox to establish a real-time simulation model of the automatic transmission system, including hydraulic system model, torque converter model, and vehicle dynamics model [33]. Matsumura et al. built a complete set of the TCU hardware-in-the-loop test system, including software and hardware platforms. The software platform consisted of clutch control, shift control, pressure control system, troubleshooting system, and other components, while the hardware platform included a control unit, actuator, interface module, fault simulation, and other sensors [34]. Brendecke and Küçükay used the dSPACE real-time platform for testing the real TCU [35]. Yan et al. used a real-time vehicle model simulation platform to transmit signals and communicate with the TCU, connecting the actual actuator with the TCU to constitute a hardware-in-the-loop test system [36–38]. Oh et al. used a real-time simulation platform to establish a transmission model of the CVT and conducted the TCU hardware-in-the-loop test, including speed ratio changing model, torque converter lock-up control model, and system pressure control model [39]. In fact, the key element of the hardware-in-the-loop simulation is to establish an accurate controlled object model, but this problem has been rarely discussed in the above literatures; specifically when the actuator model of the controlled object is more complex, it can directly affect the reliability of the test result. Currently, the hardware-in-the-loop test of the actuator model for CVTs has not been reported.

Moreover, the rapid control prototyping is an efficient way to validate the rationality of the control algorithm by connecting a virtual controller with a real controlled object. Steiber et al. established an electrical-controlled transmission test rig, the driving motor simulated the engine, the load motor simulated the driving resistance and vehicle inertia, and they used GT-power transmission and AMESim to establish the transmission model [40, 41]. Hann used the CarSim to establish the vehicle model, developing a hardware-in-the-loop test platform of the transmission based on real-time RT-LAB platform and QNX real-time operating system [42]. Sun et al. adopted the dSPACE real-time platform for the experimental study on the TCU rapid control prototyping of the CVT [43]. Yang and Zhao used the xPC Target real-time simulation platform and Dymola modeling to build a transmission model for the rapid control prototyping [44]. In summary, the current rapid control prototyping test structures usually can be put into two categories: one is to build a complete transmission system to simulate the actual driving condition. However, this type of structure is a complex one with high cost and large power consumption. The other one is only to be designed to place the specific actuator into the control loop for a simple structure, but it does not reflect the coupling between various components and the operating characteristics of the entire transmission system. Combining the advantages of both structures and proposing a new structure are of good significance.

In addition, the purpose of the above rapid control prototyping is to simulate the controlled object or the controller. However, the controlled object usually has many components, and controller usually has the multiple functions. So, it is reasonable to consider that some parts and control functions can be replaced by the real-time hardware. Turbett et al. established an electrical-controlled transmission test rig, studying engine simulation, inertia simulation, driving resistance simulation, and building the semiphysical simulation platform of the transmission [45]. Gao et al. established an electrical-controlled test rig of the CVT, the test control software can achieve driver simulation and load simulation, and the test bench used a real TCU [46]. Except for the running resistance model based on road test data, the authors considered the disturbance torque compensation to improve the accuracy and dealt with it after acquiring the road test data; they achieved this target on the test bench. To some extent, this can be an effective substitute for the road test, reducing the test cost and improving the test efficiency. Katsu and Matsumura constituted the TCU test platform of the CVT by host computer, real-time hardware platform, actuator, and signal interface circuit [47]. On the basis of the Delphi virtual vehicle hardware-in-the-loop test

platform, Zheng et al. used the OPAL-RT test drive real-time simulation system to construct the hardware-in-the-loop model and study the control strategy and algorithm of the AT transmission [48, 49].

In all, depending on different purposes and objects of the test, the structure of the hardware-in-the-loop systems can be different accordingly, but the core of the structure is always the same, namely, to simulate the control unit and the controlled object. For the newly proposed DBVCVT, according to the authors' best knowledge, there is no research on the development of a test rig of any DBVCVT system in the open literature. So, this work for the first time develops a hardware-in-the-loop test rig with the fabrication of a new prototype of DBVCVT, providing a test platform for further study on the transmission performance and the control system of the DBVCVT. In this development, to overcome disadvantages of conventional test rig of the CVT such as complex structure, high cost, and large power consumption, this work replaces the engine and load equipment with the AC motor and magnetic powder dynamometer in the test rig of the DBVCVT for a simpler structure and lower cost and power consumption. To validate the feasibility and analyze the transmission performance of the DBVCVT system more precisely, this work also validates an analytical model which was previously proposed by authors for the DBVCVT. This newly validated analytical model can also be used to design an advanced DBVCVT control system for future study, which aims at improving the system reliability, durability, and efficiency. Moreover, further experimental study is compared with the analytical model to collectively analyze the transmission performance of the DBVCVT and provide a foundation for further modelling, simulation, and control.

## 2. Proposed DBVCVT Design and Implementation

Figure 3 depicts the schematic design of the proposed DBVCVT whose principle is similar to single-belt Van Doorne's CVT (SBVCVT) because it consists of two identical single-belt Van Doorne's CVT systems and a synchronous mechanism. Figure 4 shows the experimental setup of the prototype DBVCVT and its test rig. Each single-belt Van Doorne's CVT in Figure 4 is used for the class of 660 cc automobiles with maximum input torque of 88 N·m [50]. Apparently, there are four groups of variable pulleys and two steel V-belts. At input shaft, pulleys 3, 4, 7, and 8 rotate with the input shaft synchronously. Pulleys 4 and 8 can be moved transversely by a primary synchronous shift fork, while pulleys 3 and 7 are immovable axially and coupled with the input shaft. Besides, there is a DC servo motor and a power screw mechanism to push or pull the primary synchronous shift fork so as to change the working radii of the primary pulleys. For extreme heavy-duty applications, the DC motor actuation system could be replaced with the electrohydraulic actuation system. At output side, pulleys 1, 2, 5, and 6 rotate with the two input shafts of an inverse differential gearbox, respectively. Similarly, pulleys 1 and 5 can also be moved axially by a secondary synchronous shift fork. Pulleys 2 and 6 are immovable axially and coupled with the two input shafts of the inverse differential gearbox, respectively, and then the final output is the output shaft of the inverse differential gearbox.

Theoretically, the primary and secondary pulleys and the belts are rotated simultaneously because the two groups of the primary pulleys are connected with the same input shaft, but the speeds of the belts may not be consistent due to wearing problem and manufacturing tolerances. As a result, more power loss can be produced if all the secondary pulleys are connected with the same output shaft. Hence, an inverse differential gearbox is proposed to install in the DBVCVT in order to solve this asynchronous problem, which can enter two different speeds and output an average speed of the inputs. The load cell in Figure 3 is employed to measure the spring force which provides the axial clamping forces of both primary and secondary pulleys. In fact, the slip is unfavorable to the CVT system [51], so this spring force is fed to the DBVCVT controller as a feedback signal to avoid the slip. The detailed research about the DBVCVT control will be presented in the future research paper.

In order to change the working radii of the secondary pulleys, the DC servo motor with a power screw mechanism is also used to push or pull the secondary synchronous shift fork. The primary and secondary synchronous shift forks are used for varying the widths of all the pulleys consistently to ensure the synchronous motion of the two SBVCVT systems. If the widths of the two primary or secondary pulleys in the same axle can be the same, the same belt positions can be obtained. In other words, the same clamping force on the pairs of primary or secondary pulleys can be ensured. Moreover, an extremely strong spring is installed between the power screw mechanism and the secondary shift fork. The spring is used to not only prevent the metal V-belts from damage but also provide the axial clamping force for pulleys.

In Figure 3, the electronic control unit (ECU) receives all the signals including engine load and vehicle speed signals, and then it sends the control signal to drive the DC servo motors. For example, when the engine load is considered to be constant and the increase of vehicle speed is detected by the ECU, servo motors can actuate the primary and secondary synchronous shift forks, forcing the primary pulleys to be pushed while forcing the secondary pulleys to be released or held so as to not only achieve higher transmission ratio or overdrive mode but also maintain the engine speed in an optimal operation line to achieve fuel economy. With the changes of the pulley widths, the metal V-belts are forced to move outward on the primary pulleys and inward on the secondary pulleys due to the wedge surfaces of the pulleys. Since the lengths of the two V-belts are constant, the working diameters of the primary pulleys increase while the ones of the secondary pulleys correspondingly decrease. Also, when the vehicle is running at a high transmission ratio and starts to climb up a slope, the driver will usually depress the throttle to accelerate the vehicle. As the vehicle speed tends to decrease, the ECU actuates the primary and secondary synchronous shift forks to change the transmission ratio toward a lower level. Therefore, the working diameters of the primary pulleys

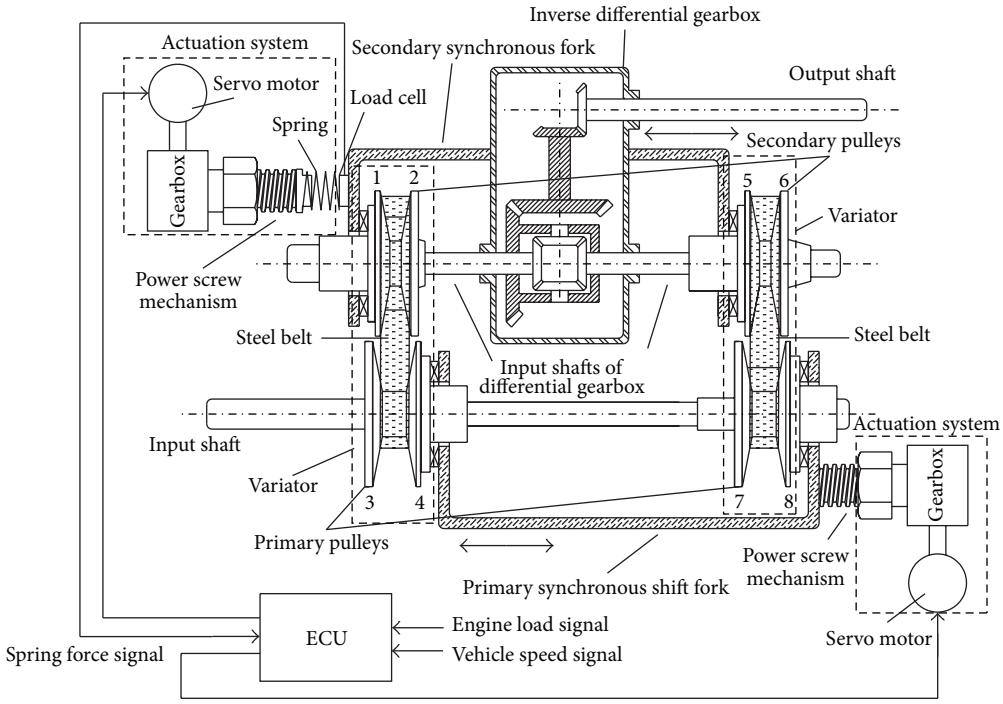


Figure 3: Schematic design of DBVCVT.

become smaller while the ones of the secondary pulleys become bigger correspondingly. All the control actions rely on a lookup table stored in the ECU, but its details are not presented in the paper because of the limited length of the paper.

In all, the test rig of the DBVCVT developed by the authors can be used to measure the speed ratio, slip, and transmission efficiency of DBVCVT. The next section considers the basic performance test of the DBVCVT based on this test rig.

## 3. Experimental Studies on DBVCVT

Since the DBVCVT is a new concept, the reason for building the above test rig is to prove the working principle of the DBVCVT. Also, authors previously developed an analytical model of the DBVCVT [29]; naturally experimental studies of this work are aimed at validating the analytical model and further analyzing the transmission performance by the following basic performance tests of the DBVCVT: the actuator performance test, the speed ratio change test, and the transmission efficiency test. As for the actuator performance, the DBVCVT is electronically controlled by same actuators used for the system clamping force and the speed ratio, respectively. So, this paper studies the characteristics of the actuator in the speed ratio test. Moreover, the speed ratio change is an important issue in the CVT. In order to achieve the good speed ratio change, it is necessary to study the characteristics of the speed ratio change. For DBVCVT, if the changing rate of the speed ratio is expressed by an empirical formula from the test data, there are a lot of experiments required to derive this formula. It is possible to be unreliable and less universal due to specific test conditions. Therefore, this paper considers the analytical model based on the complex mechanism of the DBVCVT to describe the speed ratio change [29] and the implementation of the speed ratio test can be compared with this analytical model to reliably analyze the speed ratio change. Besides, the transmission efficiency is the most important indicator in the overall performance, and yet the obvious disadvantage of conventional CVTs is the lower transmission efficiency. In the speed ratio test, this paper also analyzes the transmission efficiency in the analytical model and test rig in order to improve the transmission efficiency and provide a reference to improve the design of the DBVCVT.

It is worth mentioning that the basic performance test of the DBVCVT in this work includes the reliability test. Usually, the complete reliability test of the DBVCVT should include the reliability of the driving AC motor, the reliability of the energy absorbing dynamometer, and the reliability of the actuator system. In fact, since the DC servo motor is a key component of the electromechanical system, its reliability test should include the life test and the operational reliability test. Moreover, the whole reliability of the DBVCVT should ensure that, during the designed life, the system can meet the requirement of the torque capacity suitable for the normal operation. In addition, one parameter is directly related to the slip ratio, which can reflect the stability of the friction coefficient and the wear problem. However, this complete reliability test takes a long time to run many times and is a type of destructive testing. So, this work is limited to experimental conditions and therefore simplifies the reliability test. Similarly, as for the driving cycle test, the method for the comprehensive transmission performance test should be


Figure 4: Experimental setup of prototype DBVCVT and test rig. a. DC servo motor controllers; b. DC servo motor (secondary pulleys); c. worm gearbox of DC servo motor (secondary pulleys); d. power screw mechanism (secondary pulleys); e. integral torque and speed sensors; f. three-phase AC motor; g. spring; h. load cell (secondary pulleys); i. variator 1; j. variator 2; k. inverse differential gearbox; l. load cell (primary pulleys); m. power screw mechanism (primary pulleys); n. worm gearbox of DC servo motor (primary pulleys); o. DC servo motor (primary pulleys); p. flywheel; q. magnetic powder dynamometer; r. input shaft; s. output shaft; t. synchronous shift fork (secondary pulleys); u. synchronous shift fork (primary pulleys); v. dynamometer controller; w. control program; x. programmable ECU; y. inverter for AC motor; z. LVDT sensor.

carried out with the driving cycle test. In this paper, the test rig is included in the simulation loop, with an AC motor and a dynamometer instead of a small engine and load equipment. In order to achieve the purpose of this experiment, this work does not include the driving cycle test because the simulation of the driving cycle needs to establish the transmission model of a whole vehicle.

*3.1. Reliability Test.* The test rig of the DBVCVT was operated by the authors for several hours, the oil temperature sensor showed about 44°C during the whole test, and there was no obvious damage and scratch in the overall system, which shows that the DBVCVT has a good operational reliability and stable frictional coefficient.

*3.2. Speed Ratio Test.* From the working principle of the DBVCVT, the speed ratio change depends on the axial movements of the primary and secondary pulleys, which is achieved by the rotational degrees of two DC servo motors. The rotation of the DC servo motor changes the axial position of the pulley through the power screw mechanism. In the speed ratio test, this paper aims to develop the relationship between the rotation degree of the DC servo motor and the axial position of the pulley.

With the consideration of the slip, the speed ratio under load also named the geometric ratio can be defined as

$$i_g = \frac{r_s}{r_p}. \tag{1}$$

The speed ratio under no load can be defined as

$$i = \frac{\omega_p}{\omega_s}. \tag{2}$$

The slip ratio can be defined as

$$\varepsilon = 1 - \frac{\omega_s}{\omega_p} i_g. \tag{3}$$

The input and output speeds can be, respectively, measured by two speed sensors which is a 60-toothed magnetic pickup; then the speed ratio under no load can be obtained from (2). From (3), it is noted that the key to measure the slip is to determine the geometric ratio $i_g$. In this paper, by measuring the axial displacements of the primary and secondary pulleys, the corresponding geometric ratio $i_g$ can be calculated. This is accomplished by installing two linear variable differential transformers (LVDT). Since the special transmission mechanism of the DBVCVT determines the belt to move inward or outward along the pulleys when shifting, the radical and axial movements of the belt can cause the axial misalignment of the belt due to the fixed length of the belt, as shown in Figure 5. This axial misalignment of the belt can affect the transmission efficiency and speed ratio [29] and it is necessary to develop the analytical model of the speed ratio based on the axial misalignment of the belt.

When developing the test rig, the authors need to ensure there is no axial misalignment of the belt under $i_{g,0} = 1$. Meanwhile, the symmetric center lines between the primary pulley and the secondary pulley coincide, so the working radius of the primary pulley under $i_{g,0} = 1$ can be shown as

$$r_p = r_0. \tag{4}$$

The corresponding working radius of the secondary pulley under $i_{g,0} = 1$ can be shown as

$$r_s = i_{g,0} \cdot r_p = r_0. \tag{5}$$

In Figure 5(a), when the belt on the primary pulley moves inward, the movable primary pulley moves left and the corresponding axial moving displacement of the primary pulley measured by primary LVDT in Figure 4 can be regarded as

$$\Delta r_p = 2\left(r_0 - r_p\right) \tan\theta_p. \tag{6}$$

Then, the working radius of the primary pulley can be shown as

$$r_p = r_0 - \frac{\Delta r_p}{2\tan\theta_p}. \tag{7}$$

At the same time, the belt on the secondary pulley moves outward, the movable secondary pulley moves right, and the

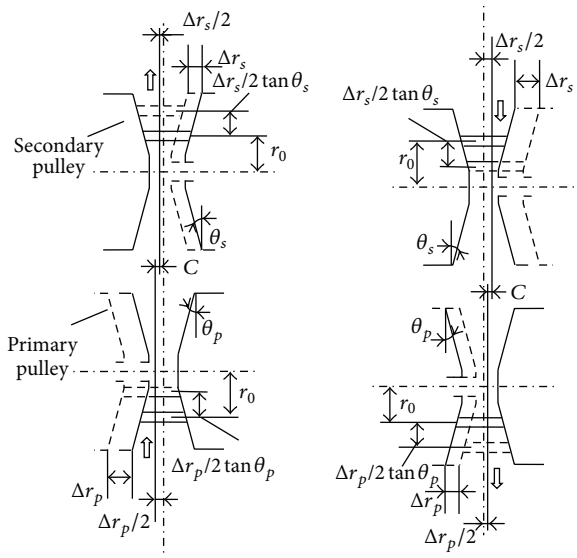


(a) Speed ratio increases (b) Speed ratio decreases

Figure 5: Axial misalignment of belt when shifting.

corresponding axial moving displacement of the secondary pulley measured by secondary LVDT in Figure 4 can be regarded as

$$\Delta r_s = 2\left(r_s - r_0\right)\tan\theta_s. \tag{8}$$

Then, the working radius of the secondary pulley can be shown as

$$r_s = r_0 + \frac{\Delta r_s}{2\tan\theta_s}. \tag{9}$$

The speed ratio increases and can be defined as

$$i_g = \frac{r_0 + \Delta r_s/2\tan\theta_s}{r_0 - \Delta r_p/2\tan\theta_p}. \tag{10}$$

In Figure 5(b), when the belt on the primary pulley moves outward, the movable primary pulley moves right and the corresponding axial moving displacement of the primary pulley measured by primary LVDT in Figure 4 can be regarded as

$$\Delta r_p = 2\left(r_p - r_0\right)\tan\theta_p. \tag{11}$$

Then, the working radius of the primary pulley can be shown as

$$r_p = r_0 + \frac{\Delta r_p}{2\tan\theta_p}. \tag{12}$$

At the same time, the belt on the secondary pulley moves inward, the movable secondary pulley moves left, and the corresponding axial moving displacement of the secondary pulley measured by secondary LVDT in Figure 4 can be regarded as

$$\Delta r_s = 2\left(r_0 - r_s\right)\tan\theta_s. \tag{13}$$

Then, the working radius of the secondary pulley can be shown as

$$r_s = r_0 - \frac{\Delta r_s}{2\tan\theta_s}. \tag{14}$$

The speed ratio decreases and can be defined as

$$i_g = \frac{r_0 - \Delta r_s/2\tan\theta_s}{r_0 + \Delta r_p/2\tan\theta_p}. \tag{15}$$

From Figure 5, the axial misalignment of the belt can be defined as

$$C = \left(2r_0 - r_p - r_s\right)\tan\theta_p = \left(2r_0 - r_p - r_s\right)\tan\theta_s. \tag{16}$$

Using (10) and (15), (16) can then be shown as

$$C = \frac{4r_0^2\left(i_g - 1\right)^2}{\pi a\left(i_g + 1\right)^2}\tan\theta_p = \frac{4r_0^2\left(i_g - 1\right)^2}{\pi a\left(i_g + 1\right)^2}\tan\theta_s. \tag{17}$$

Due to the fact that the axial movement of the pulley is driven by the DC servo motor, the relationship between the axial movement of the primary pulley and the rotational degree of the DC servo motor can be defined as [52]

$$\frac{2\pi}{S_w} = \frac{\theta_{mp}}{\Delta r_p i_w}, \tag{18}$$

where $S_w$ is the pitch of screw thread, $i_w$ is the speed ratio of gearbox, and $\theta_{mp}$ is the rotational degree of primary DC servo motor.

Similarly, the relationship between the axial movement of the secondary pulley and the rotational degree of the DC servo motor can be defined as

$$\frac{2\pi}{S_w} = \frac{\theta_{ms}}{\Delta r_s i_w}, \tag{19}$$

where $\theta_{ms}$ is the rotational degree of secondary DC servo motor.

The primary clamping force of the DBVCVT is adjusted by the DC servo motor and measured by the load cell of the primary pulleys as shown in Figure 4. The relationship between the total primary clamping force for an $n$-belt Van Doorne's continuous variable transmission (VCVT) system and the DC servo motor is

$$Q_{p,n} = \frac{2T_{mp}i_w}{d_w \tan(\lambda_w + \rho_w)}, \tag{20}$$

where $T_{mp}$ is the driving torque of primary DC servo motor, $d_w$ is the mean diameter of screw thread, $\lambda_w$ is the lead angle of screw thread, and $\rho_w$ is the equivalent friction angle [52].

The secondary clamping force of the DBVCVT is adjusted by the DC servo motor and measured by the load cell of the secondary pulleys as in Figure 4. The relationship between the total secondary clamping force for an $n$-belt VCVT system and the DC servo motor is

$$Q_{s,n} = \frac{2T_{ms}i_w}{d_w \tan(\lambda_w + \rho_w)} + K_{\text{spring}}\Delta r_s + F_{\text{pre}}, \tag{21}$$

where $T_{ms}$ is the driving torque of secondary DC servo motor, $K_{\text{spring}}$ is the spring stiffness, and $F_{\text{pre}}$ is the preload spring force. As mentioned before, the DBVCVT is composed of two combined individual SBVCVT systems, so $n$ can be set to be 2 for the DBVCVT system and to be 1 for the SBVCVT.

Moreover, the working length of the steel belt can be calculated with

$$L = r_p(\pi + 2\alpha) + r_s(\pi - 2\alpha) + 2a\cos\alpha. \tag{22}$$

Based on (1)~(22), the speed ratio $i_g$ can be obtained. As the analytical model of the DBVCVT has been previously proposed by the authors in a conference paper [29], the required axial clamping forces of primary and secondary pulleys under high transmission ratio ($i < 1$) and low transmission ratio ($i \geq 1$) can be obtained. Due to the limited page, the analytical model of the DBVCVT is not mentioned in this paper. Besides, the parameters used in the simulation tests are shown in Table 1 in which the geometrical and mechanical parameters come from the prototype DBVCVT presented in Section 2, experiments, handbooks, and manufacturer catalogues. The prototype is designed based on the components of an existing 600 cc automobile. Regarding the sources of the parameters, $K$, $\eta_{dt}$, $\eta_d$, $\mu_{\text{ep}}$, and $\mu_{\text{re}}$, they are presented in Section 3.3 and the analytical model of DBVCVT in [29]. It is worth mentioning that the value of the sliding angle $\gamma$ in Table 1 is assumed to be 90°, because Kim and Lee experimentally found that along the contact angle, the radial motion between the steel elements and the pulley only varies about $10^{-4}$~$10^{-3}$ mm, which can be neglected as compared to the tangential motion [12].

In fact, the transmission efficiency and ratio accuracy decreases when the axial misalignment of the belt $C$ increases [53]. In the DBVCVT, the axial moving displacements of the pulleys $\Delta r_p$ and $\Delta r_s$ are controlled by two actuator systems. One can provide the required system clamping force; the other can rotate without load to push or pull the system. Although the synchronization control of two DC servo motors is simple, the DBVCVT is at the risk of increasing the axial misalignment. So, the use of the independent control is better than the former. In order to achieve the accurate speed ratio control, the relationship between the speed ratio and the rotational degree of the primary DC servo motor is necessary to be ensured. In the test, the authors first set the initial position of the DBVCVT and then change the rotational degree of the primary DC servo motor. By measuring the axial moving displacements of the pulleys $\Delta r_p$ and $\Delta r_s$ and calculating the speed ratio by (15), the relationship between the speed ratio and the rotational degree of the primary DC servo motor is obtained in Figure 6. By comparing the simulation result using the analytical model with the experimental result based on the test rig, they are in a good agreement and the proposed analytical model is valid. One conclusion is that using the analytical model can adjust the speed ratio by controlling the rotational degree of the primary DC servo motor.

In fact, the control of the DBVCVT is essentially the control of the clamping forces. In the DBVCVT, the axial clamping force of the primary pulley $Q_{p,2}$ controls the speed ratio while the axial clamping force of the secondary pulley $Q_{s,2}$ controls the slip. In the analytical model of the DBVCVT,

Table 1: Parameters of analytical model and prototype of DBVCVT.

| | | | | | | | |
|---|---|---|---|---|---|---|---|
| $a$ | 195 mm | $h$ | 2 mm | $m_e$ | 0.005 kg | $\eta_{\text{dt}}$ | 0.96 |
| $B$ | 100 mm | $h_e$ | 2 mm | $N_r$ | 12 | $\theta_p$ | 11° |
| $C_e$ | 2 kg/m | $h_r$ | 0.185 mm | $S_w$ | 5 mm | $\theta_s$ | 11° |
| $C_r$ | 0.04 kg/m | $i_w$ | 30 : 1 | $\nu_b$ | 40 mm$^2$/s | $\lambda_w$ | 4.25° |
| $d_b$ | 70 mm | $K$ | 5.5 mm | $\gamma$ | 90° | $\mu_{\text{ep}}$ | 0.001 |
| $d_w$ | 21.5 mm | $K_t$ | 0.52 | $\varepsilon$ | 0 | $\mu_{\text{re}}$ | 0.07 |
| $f_b$ | 0.7 | $L$ | 598 mm | $\eta_d$ | 0.9 | $\rho_w$ | 11.69° |

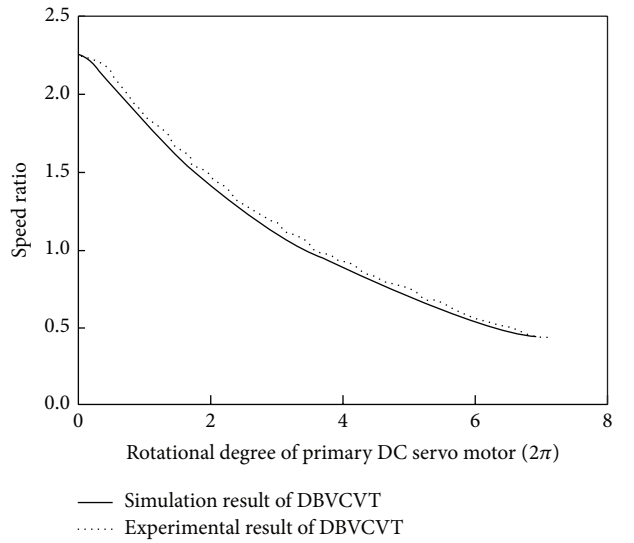


Figure 6: Relationship between speed ratio and rotational degree of primary DC servo motor.

the speed ratio change is derived by the input torque, input speed, target speed ratio, and primary and secondary clamping forces. This paper implements the following speed ratio test in order to study the above relationship between the primary clamping force and the speed ratio.

As the analytical model of the DBVCVT has been previously proposed by the authors in a conference paper [29], it is known that the axial clamping forces for an $n$-belt VCVT system are functions of input torque and speed ratio. In other words, different axial clamping forces are required for various combinations of input torque and input speed. The combination makes the experiments very complicated. To reduce the number of combinations of variables in the experiments, the whole test process of the DBVCVT is set as follows. First of all, the authors set a fixed input torque coupled with four different input speeds, respectively. Then, when the prototype DBVCVT runs under the maximum input speed and maximum speed ratio, the authors set a fixed excessive secondary clamping force for this fixed input torque. Hence for the most part, the selection of this excessive secondary clamping force can minimize the slippage of the prototype DBVCVT under this fixed input torque, different input speeds, and speed ratios. In Figure 4, this excessive secondary clamping force can be measured by the load cell in the secondary pulleys. Under this fixed excessive secondary clamping force and input torque, when the input speed changes, the authors only adjust the primary clamping force to change the speed ratio between the maximum speed ratio and the minimum speed ratio. Finally, the authors measure the speed ratio variation along with the corresponding primary clamping force under different excessive secondary clamping forces, input speeds, and input torque. Table 2 shows test conditions. In order to exam the performance of the DBVCVT system, the simulation of the DBVCVT system under the same excessive secondary clamping forces, input torque, full-range speed ratio, input speeds, and the parameters in Table 1 was also conducted. To ensure a fair comparison under the same conditions, the excessive secondary clamping forces in Table 2 were applied to the prototype DBVCVT and the simulation at the same time.

Moreover, the performances of DBVCVT and SBVCVT are also compared. To ensure a fair comparison, the dimensions and the other parameters of the SBVCVT are the same as one of single-belt CVT systems in the DBVCVT, except the number of belts. Since the torque capacity of the DBVCVT is shared by two combined individual SBVCVT systems [29], it is necessary to mention that, for fairly comparing SBVCVT and DBVCVT under the same input torque $T_{i,1} = T_{i,2} = T_i$, input speed $n_i$, and full-range speed ratio $i_g$, the excessive secondary clamping forces for the prototype SBVCVT should be set equal to the excessive secondary clamping forces for the prototype DBVCVT, which means $Q_{s,1} = Q_{s,2} = Q_s$. Similarly, the simulation of the SBVCVT system under the same excessive secondary clamping forces, input torque, full-range speed ratio, input speeds, and the parameters in Table 1 was also conducted. In addition, the excessive secondary clamping forces in Table 2 were also applied to the prototype SBVCVT and the simulation at the same time.

To demonstrate the outstanding performance of the DBVCVT, the authors set a fixed excessive secondary clamping force $Q_{s,2} = 40000$ N for a fixed high driving torque $T_{i,2} = 107.6$ N·m in Table 2. As mentioned before in Section 2, each single-belt Van Doorne's CVT in Figure 4 is used for the class of 660 cc automobiles with maximum input torque of 88 N·m [50], so this test condition is not applicable to the SBVCVT. In this paper, only the prototype DBVCVT and the simulation under this excessive secondary clamping force $Q_{s,2} = 40000$ N, input torque $T_{i,2} = 107.6$ N·m, full-range speed ratio, and input speeds was conducted.

Figures 7(a)–7(c) show the experimental results of speed ratio responses of DBVCVT and SBVCVT based on the test rig and their simulation results based on the analytical model under $n_i = 500$ RPM and $T_i = 25.3$ N·m, 54.3 N·m, and 78.8 N·m, respectively. Figure 7(d) shows the comparison of simulation and experimental results of speed ratio response of DBVCVT under $n_i = 500$ RPM and $T_{i,2} = 107.6$ N·m. Figures 8(a)–8(c) show the experimental results of speed ratio responses of DBVCVT and SBVCVT based on the test rig and their simulation results based on the analytical model under $n_i = 800$ RPM and $T_i = 25.3$ N·m, 54.3 N·m, and 78.8 N·m, respectively. Figure 7(d) shows the comparison of simulation and experimental results of speed ratio response of DBVCVT under $n_i = 800$ RPM and $T_{i,2} = 107.6$ N·m. Figures 9(a)–9(c) show the experimental results of speed ratio responses of DBVCVT and SBVCVT based on the test rig and their simulation results based on the analytical model under $n_i = 1200$ RPM and $T_i = 25.3$ N·m, 54.3 N·m, and 78.8 N·m, respectively. Figure 9(d) shows the comparison of simulation and experimental results of speed ratio response of DBVCVT under $n_i = 1200$ RPM and $T_{i,2} = 107.6$ N·m. They have a good agreement under different test conditions, respectively, which means that the analytical model can effectively predict the dynamic characteristics and correctly describe the transmission performance of the proposed DBVCVT at different transmission conditions. Moreover, the evaluation of the experimental and simulation results can lead to the following useful conclusions for the novel DBVCVT.

(1) By comparing the simulation results using the analytical model with the experimental results based on the test rig, there are some minor differences. It is because the analytical model is developed by ignoring some factors, such as pulley deformations and friction of synchronous shift fork, which can cause the minor simulation errors. As a result, the primary clamping force required to achieve the same speed ratio in the experiment is higher than the primary clamping force in the simulation. In addition, it is observed that the experimental results are scattered because of some factors, such as sensor noise and test rig vibration due to manufacturing error. Despite these minor errors, Figures 7–9 show that the overall simulation results are in a good agreement with the experimental results, which means that the working principle in the analytical model is validated and this analytical model can be used with the test rig to analyze the transmission performance of the DBVCVT at different transmission conditions.

(2) In order to analyze the effect of the primary clamping force on the speed ratio response, Figures 7–9 show the

Table 2: Test conditions.

| Full-range speed ratio $i_g$ | Input speed $n_i$ (RPM) | Input torque (N·m) | Excessive secondary clamping force (N) |
|---|---|---|---|
| 0.44–2.25 | 500, 800, 1200 | $T_i$ = 25.3 N·m | $Q_s$ = 10000 N |
| | | $T_i$ = 54.3 N·m | $Q_s$ = 20000 N |
| | | $T_i$ = 78.8 N·m | $Q_s$ = 30000 N |
| | | $T_{i,2}$ = 107.6 N·m | $Q_{s,2}$ = 40000 N |

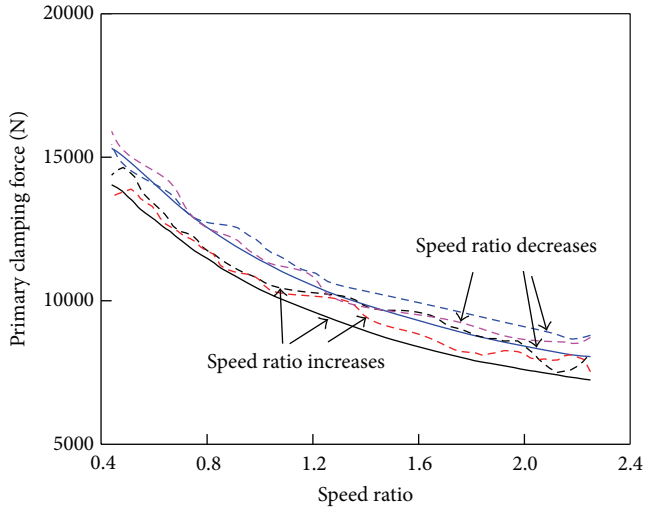


(a) $n_i$ = 500 RPM, $T_i$ = 25.3 N·m

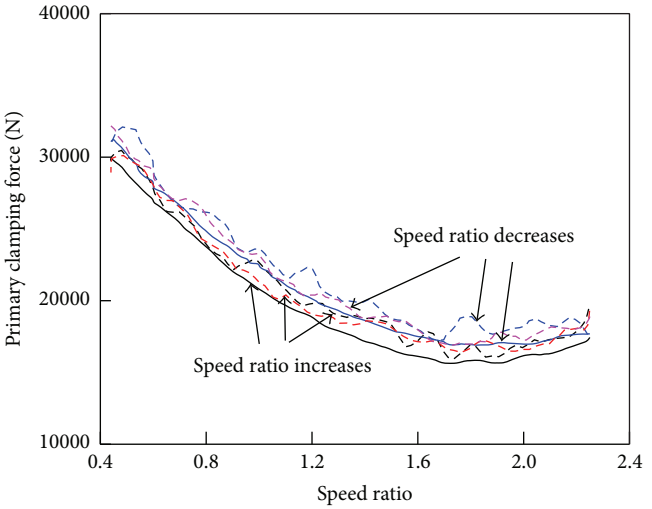


(b) $n_i$ = 500 RPM, $T_i$ = 54.3 N·m

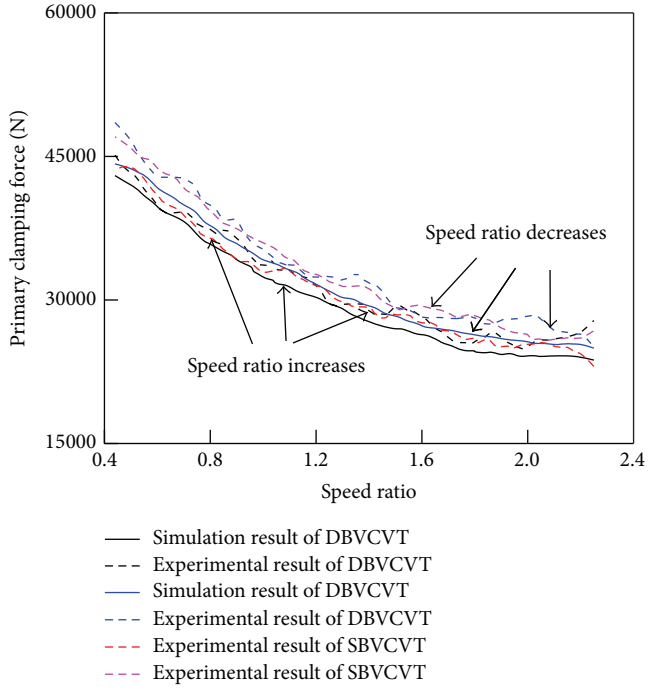


(c) $n_i$ = 500 RPM, $T_i$ = 78.8 N·m

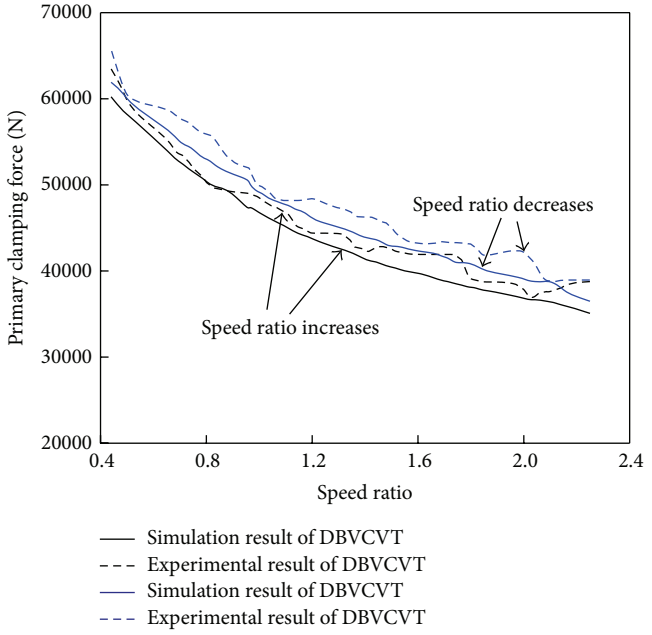


(d) $n_i$ = 500 RPM, $T_{i,2}$ = 107.6 N·m

Figure 7: Comparison of simulation and experimental results of speed ratio responses under $n_i$ = 500 RPM.

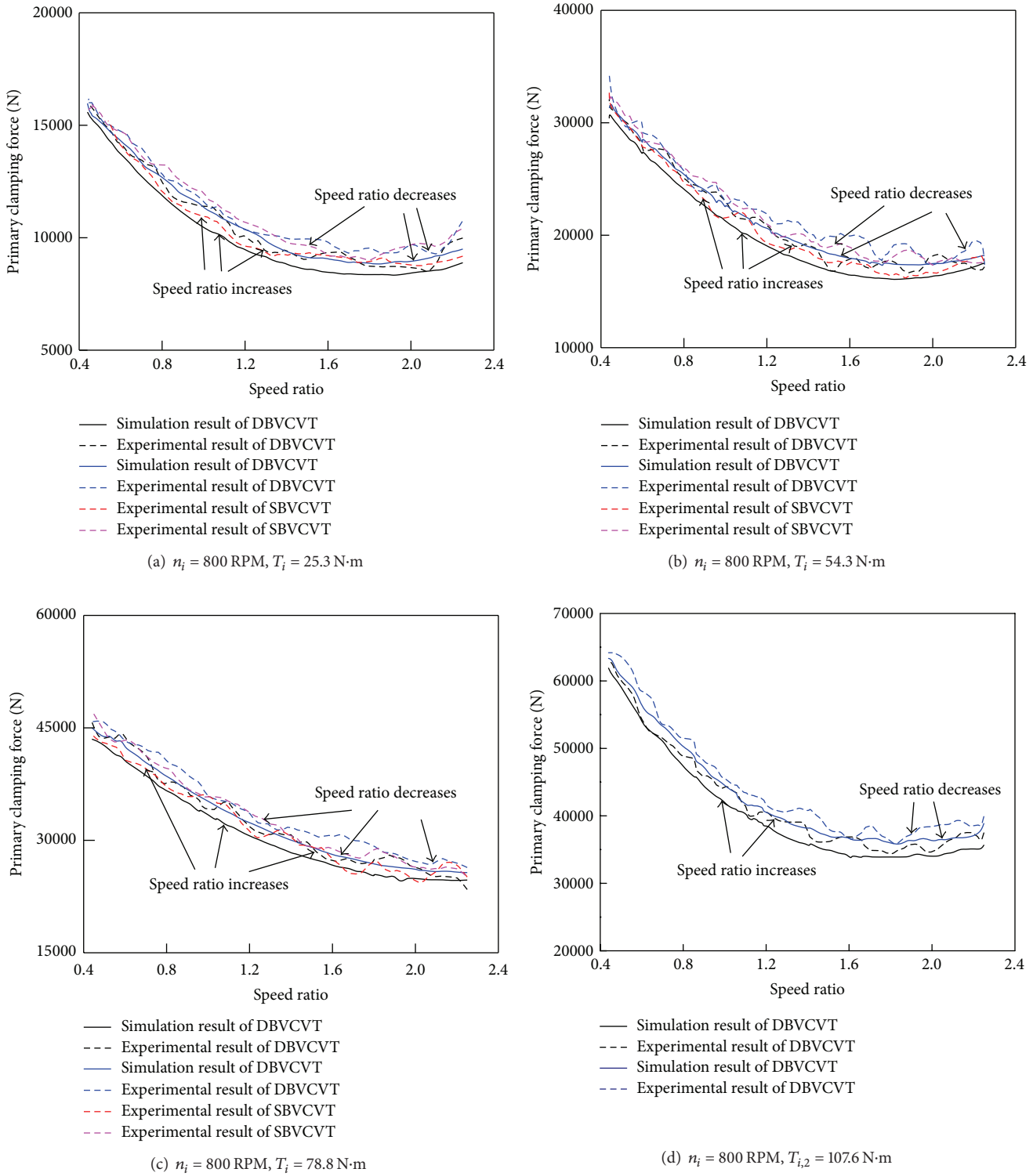


FIGURE 8: Comparison of simulation and experimental results of speed ratio responses under $n_i$ = 800 RPM.

comparison of simulation and experimental results of speed ratio response of DBVCVT under different test conditions. It is noted that when the speed ratio increases or decreases, there are some obvious differences in the corresponding simulation or experimental results of the primary clamping force. The changing process of the primary clamping force when the speed ratio decreases is higher than the changing process of the primary clamping force when the speed

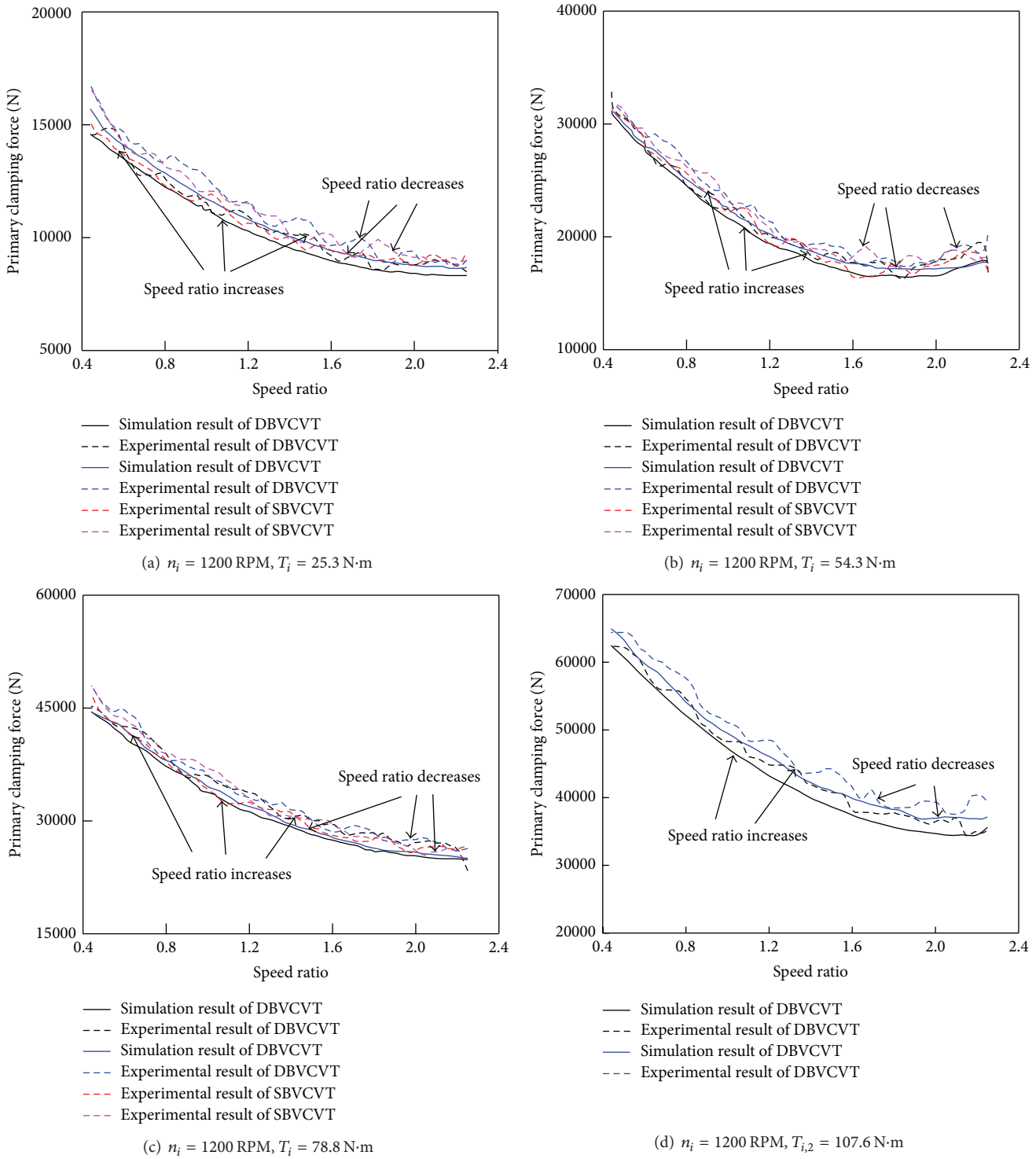


Figure 9: Comparison of simulation and experimental results of speed ratio responses under $n_i$ = 1200 RPM.

ratio decreases. It is believed that this difference is caused by the hysteresis of the primary clamping force in belt-type CVTs. When the speed ratio changes, the DBVCVT actually shifts from one steady state to the dynamic state first and then shifts to another steady state. Obviously, during this special transition, the changing rate of the speed ratio cannot synchronously follow the changing rate of the primary clamping force. To be exact, the changing rate of the speed ratio is behind the changing rate of the primary clamping force. It is because the dynamic interactions between the belt and the pulleys are different under high transmission ratios ($i < 1$) and low transmission ratios ($i \geq 1$). In fact, the

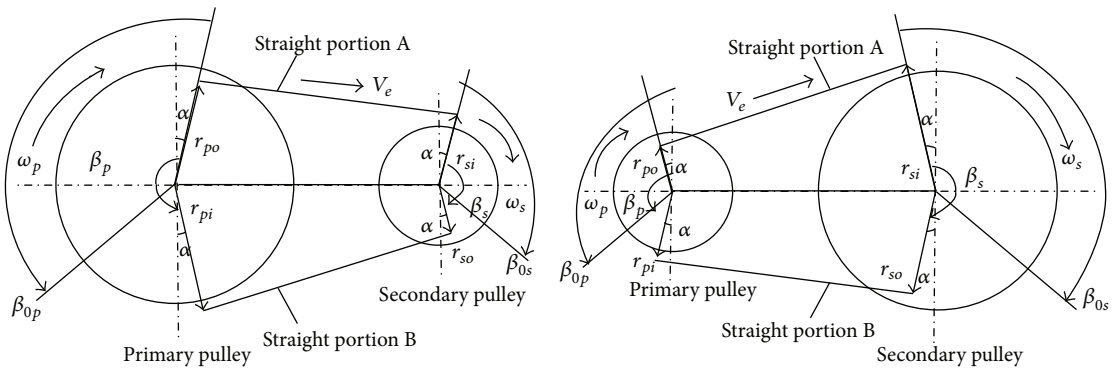


Figure 10: Actual belt positions of DBVCVT.

whole shifting mechanism is the same, but the directions of radial friction between steel element and primary pulley $F_{rp}$ and radial friction between steel element and secondary pulley $F_{rs}$ are different under $i < 1$ and $i \geq 1$. When the speed ratio increases, the $F_{rp}$ increases but is still the static friction and the belt actually cannot move along the radial direction. Once the $F_{rp}$ becomes the sliding friction, the belt begins to move inward along the radial direction and shifts, while the $F_{rp}$ moves outward. Similarly, when the speed ratio decreases, the $F_{rs}$ increases but is still the static friction and the belt actually cannot move along the radial direction. Once the $F_{rs}$ becomes the sliding friction, the belt begins to move outward along the radial direction and shifts, while the $F_{rs}$ moves inward. Furthermore, it also can be explained by the actual belt operating positions of the DBVCVT, as shown in Figure 10. By considering the radial sliding of the steel belt while travelling into or out of the pulleys, $F_{rp}$ exists at the entry of the primary pulley; then the steel element tends to leave the wedge of the primary pulley, but the combined force of the steel belt here is too small to provide a necessary inward component to overcome the radial friction. Thus, the effective radius is larger than the working radius. However, at the exit of the primary pulley, the steel element tends to stay in the wedge of the primary pulley until the system provides a sufficient outward component from the combined force in the steel belt to overcome the radial friction and hence pulls out the steel element. However, due to the principle of constant length of the steel belt, the effective radius at the entry of the secondary pulley is shifted outward the centre of the pulley and hence the effective radius is larger than the working radius. While at the exit of the secondary pulley, the belt is shifted toward the centre of the pulley and hence its effective radius is smaller than the working radius. Therefore, in the analytical model of the DBVCVT, the effective radii are considered instead of traditional working radii. In this paper, the experimental investigation shows the hysteresis of the primary clamping force and evaluates the relationship between the primary clamping force and the speed ratio in the analytical model, which is very important to the accurate speed ratio control.

(3) It is worth mentioning that, in the analytical model of the DBVCVT, the speed ratio change is derived by the input torque, the input speed, the target speed ratio, and the primary and secondary clamping forces. In this work, authors only design and implement the full-range speed ratio change under different input speeds and torques, because the primary clamping force is considered to directly change the speed ratio. In fact, the excessive secondary clamping force coupled with the input torque is set not only to eliminate the belt slippage but also to show the rationality of the test during the full-range speed ratio. It is possible to consider the secondary clamping force as an individual to analyze its impact on the full-range speed ratio change, but the test can be designed under no load. Similarly, it is possible to consider the input speed or the input torque as an individual to analyze its impact on the full-range speed ratio change, but the test design and implementation are inevitably limited and cannot reflect the vehicle's real condition. In all, the impacts of the secondary clamping force, input speed, and input torque on the speed ratio response can be ignored in this paper.

*3.3. Transmission Efficiency Test.* When testing the speed ratio, the transmission efficiency of the DBVCVT is also measured by the authors. Based on the analytical model of DBVCVT previously developed in [29], the transmission efficiency of DBVCVT can be obtained by considering some power losses. The power loss due to radial friction between the steel element and the pulley is given by

$$P_1 = \left\{\omega_p \left[F_p\left(\beta_p\right) r_{pi} - F_p\left(0\right) r_{po}\right] + \omega_s \left[F_s\left(0\right) r_{so} - F_s\left(\beta_s\right) r_{si}\right]\right\} \cdot n. \tag{23}$$

The power loss due to the tangential friction between the steel element and the pulley is considered as

$$P_2 = 0.07\varepsilon v_p \left(\frac{Q_{ps}}{\cos\left(\theta_p/2\right)} + \frac{Q_{ss}}{\cos\left(\theta_s/2\right)}\right) \cdot n. \tag{24}$$

In this paper, the excessive clamping forces are considered to minimize the slippage of prototype DBVCVT under different input speeds and full-range speed ratio. Thus, the value of $\varepsilon$ is selected as 0. Moreover, the power loss due to the

friction between inner layer of steel ring and contact surface of steel element is defined as

$$P_3 = \begin{cases} \mu_{\mathrm{re}} v_s h \left[ \dfrac{\left(C_r v_s^2 - F_A N_r\right)\left(e^{-\mu_{\mathrm{re}}\beta_s} - 1\right)}{\mu_{\mathrm{re}} N_r} \left( \dfrac{1}{r_{si}} - \dfrac{1}{r_{po}} \right) + \dfrac{\left(F_A + F_B\right)\tan\alpha}{r_{po}} \right] \cdot n, & (i < 1) \\ \mu_{\mathrm{re}} v_s h \left[ \dfrac{\left(C_r v_s^2 - F_A N_r\right)\left(e^{-\mu_{\mathrm{re}}\beta_s} - 1\right)}{\mu_{\mathrm{re}} N_r} \left( \dfrac{1}{r_{pi}} - \dfrac{1}{r_{so}} \right) + \dfrac{\left(F_A + F_B\right)\tan\alpha}{r_{so}} \right] \cdot n, & (i \geq 1). \end{cases} \tag{25}$$

The kinetic energy loss of the steel element is defined as

$$P_4 = \begin{cases} \dfrac{1}{2} m_e V_e^3 \left( \dfrac{2h \cdot r_{po} + h^2}{h_e r_{po}^2} + \dfrac{2h \cdot r_{si} + h^2}{h_e r_{si}^2} \right) \cdot n, & (i < 1) \\ \dfrac{1}{2} m_e V_e^3 \left( \dfrac{2h \cdot r_{pi} + h^2}{h_e r_{pi}^2} + \dfrac{2h \cdot r_{so} + h^2}{h_e r_{so}^2} \right) \cdot n, & (i \geq 1). \end{cases} \tag{26}$$

The power loss due to speed-dependent bearing frictional torque of the input shaft is given below:

$$P_5 = \begin{cases} \dfrac{10^{-10} \cdot d_b^3 n_i^{5/3} n \cdot f_b v_b^{2/3}}{9549}, & v_b \cdot n_i \geq 2000 \\ \dfrac{160 \cdot 10^{-10} \cdot d_b^3 f_b n \cdot n_i}{9549}, & v_b \cdot n_i < 2000. \end{cases} \tag{27}$$

The power loss due to speed-dependent bearing frictional torque of the output shaft is also given below:

$$P_6 = \begin{cases} \dfrac{10^{-10} \cdot d_b^3 n_o^{5/3} n \cdot f_b v_b^{2/3}}{9549}, & v_b \cdot n_o \geq 2000 \\ \dfrac{160 \cdot 10^{-10} \cdot d_b^3 f_b n \cdot n_o}{9549}, & v_b \cdot n_o < 2000, \end{cases} \tag{28}$$

where $n_i$ and $n_o$ are, respectively, the input speed of the primary pulley and the output speed of the secondary pulley in revolutions per minute (RPM).

In addition, the transmission efficiency of inverse differential gearbox is also considered by referring to [54]. Figure 11 shows the speed relationship of inverse differential gearbox in DBVCVT. $n_{o1}$ and $n_{o2}$ are, respectively, the output speeds of secondary pulleys 1 and 2 in revolutions per minute (RPM). $\Delta n$ in Figure 11 is the difference between $n_{o1}$ and $n_{o2}$. In fact, the efficiency of the gear train in the inverse differential gearbox $\eta_d$ is related to the structure itself. The bevel gears are used in the inverse differential gearbox, so $\eta_d$ is usually selected as 0.9 [55]. It should be noted that a lower $\eta_d$ means a larger friction loss in the differential gearbox. However, the friction loss happens only if there is a speed difference between two shafts. Generally, if this speed difference $\Delta n$ is not very large, the friction loss is not obvious. When the speeds of two shafts are the same, the friction loss is zero. Otherwise, the transmission efficiency of the inverse differential gearbox $\eta_{dt}$ can be derived as follows based on the theory of the automotive differential:

$$\eta_{dt} = K_t \left[ \eta_d \left( 1 + \frac{B}{R} \right) + \left( 1 - \frac{B}{R} \right) \right], \tag{29}$$

where $K_t$ is the torque distribution coefficient and selected as 0.52 [55]. $B$ is the distance between the centerline of steel belt and the centerline of differential gearbox and $R$ is the distance as shown in Figure 11. Obviously, $\eta_{dt}$ is determined by $B$, $R$, and $\eta_d$. In DBVCVT, the value of $R$ can be calculated by

$$R = \frac{B\left(n_{o1} + n_{o2}\right)}{n_{o1} - n_{o2}}. \tag{30}$$

In this paper, the approximation of $R$ is obtained by the experimental result of inverse differential gearbox as shown in Table 3. Table 3 also reveals that the mean value of $R$ is 38.56 m. By setting $R_{\mathrm{mean}}$ as $R$ as well as using (29) and Table 1, 0.96 is obtained for $\eta_{dt}$. As mentioned before, two sets of DC servo motors and power screw mechanisms are used to adjust the primary and secondary clamping forces. When the DC motor actuation system works for gearshift, it must overcome the friction in the power screw mechanism. It is noted that the shifting power mainly depends on the power screw efficiency, the speed, and driving torque of the DC servo motors. However in [29], the analytical model of the DBVCVT has been developed under two different steady-state cases. Actually, no shifting power is consumed because the DC servo motors are stopped at the steady-state cases. So, only the input power from the prime mover and the output load are considered to exam the transmission efficiency of DBVCVT in this paper. With reference to the design of the DBVCVT and the above sections, the power transmission efficiency based on the input power from the primary pulleys to the secondary pulleys is defined as

$$\eta_n = \frac{\eta_{dt} \cdot \left[ n_i T_{i,n} - 9549 \cdot \left( P_1 + P_2 + P_3 + P_4 + P_5 + P_6 \right) \right]}{n_i T_{i,n}} \times 100\%. \tag{31}$$

To determine the power transmission efficiency for the DBVCVT, the number of belts $n$ in (31) is set to be 2, while $n$ in (31) is set to be 1 for the SBVCVT. Besides, there is no inverse differential gear in the SBVCVT, so $\eta_{dt}$ in (31) is set to be 1 for the SBVCVT. Equations (23)~(31) are useful for

Table 3: Experimental results of inverse differential gearbox.

| | | | | Input torque $T_{i,2}$ = 150 N·m | | | |
|---|---|---|---|---|---|---|---|
| $i$ | $n_i$ (RPM) | $n_{o1}$ (RPM) | $n_{o2}$ (RPM) | Error between $n_{o1}$ and $n_{o2}$ (%) | $n_o$ (RPM) | $R$ (m) | $R_{mean}$ (m) |
| 1.46 | 500 | 342 | 342 | 0.00% | 342 | 0 | 38.56 |
| | 1000 | 686 | 684 | 0.29% | 685 | 68.5 | |
| | 2000 | 1372 | 1368 | 0.29% | 1370 | 68.5 | |
| | 3000 | 2059 | 2051 | 0.39% | 2055 | 51.38 | |
| 0.74 | 500 | 678 | 674 | 0.59% | 676 | 33.8 | |
| | 1000 | 1355 | 1347 | 0.59% | 1351 | 33.78 | |
| | 2000 | 2712 | 2694 | 0.66% | 2703 | 30.03 | |
| | 3000 | 4072 | 4036 | 0.88% | 4054 | 22.52 | |

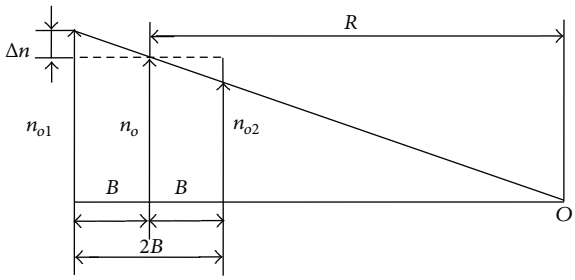


Figure 11: Speed relationship of inverse differential gearbox in DBVCVT.

system simulation. In this novel DBVCVT, the forces acting on the steel rings and the steel elements are very complicated, so only the above power losses are considered. In fact, extra power losses are necessary to be investigated deeply in the future, such as belt slip loss and pulley deflection loss.

Figures 12(a)–12(c) show the experimental results of transmission efficiencies of DBVCVT and SBVCVT based on the test rig and their simulation results based on the analytical model under $n_i$ = 500 RPM and $T_i$ = 25.3 N·m, 54.3 N·m, and 78.8 N·m, respectively. Figure 12(d) shows the comparison of simulation and experimental results of transmission efficiency of DBVCVT under $n_i$ = 500 RPM and $T_{i,2}$ = 107.6 N·m. Figures 13(a)–13(c) show the experimental results of transmission efficiencies of DBVCVT and SBVCVT based on the test rig and their simulation results based on the analytical model under $n_i$ = 800 RPM and $T_i$ = 25.3 N·m, 54.3 N·m, and 78.8 N·m, respectively. Figure 13(d) shows the comparison of simulation and experimental results of transmission efficiency of DBVCVT under $n_i$ = 800 RPM and $T_{i,2}$ = 107.6 N·m. Figures 14(a)–14(c) show the experimental results of transmission efficiencies of DBVCVT and SBVCVT based on the test rig and their simulation results based on the analytical model under $n_i$ = 1200 RPM and $T_i$ = 25.3 N·m, 54.3 N·m, and 78.8 N·m, respectively. Figure 14(d) shows the comparison of simulation and experimental results of transmission efficiency of DBVCVT under $n_i$ = 1200 RPM and $T_{i,2}$ = 107.6 N·m. Under different test conditions, the general agreement between them proves the correctness of the analytical model of DBVCVT. However, the minor difference between them depicts that the experimental results are slightly lower than the simulation results. It is because the analytical model is developed by ignoring some factors, such as pulley deformations and friction of synchronous shift fork, which can account for this minor difference. In addition, although the noises in the test rig of DBVCVT are prevented by several ways and indeed cannot be totally avoided during the whole test process, the manufacturing error and test rig vibration can also cause the noises, even some sensors used in the test rig. Therefore, the scattered experimental results are regarded as acceptable and can truly show the transmission performance of DBVCVT. From the curves in Figures 12–14, it can be observed that whether the speed ratio increases or decreases, there is no obvious difference between experimental and simulation results under all test conditions, so this work only shows the comparison of experimental results of the transmission efficiency under different test conditions. Figures 12–14 also show the comparison of experimental results of the transmission efficiency of DBVCVT under different input torques and input speeds. Table 4 shows the mean transmission efficiency of the experimental results of the DBVCVT under different test conditions. These detailed comparison of the experimental and simulation results in Figures 12–14 and Table 4 can lead to the following discussion about the transmission performance for the novel DBVCVT.

(1) First, the transmission efficiency of prototype DBVCVT shown in Figures 12–14 is below 70%. Moreover, Figures 12(a)–12(c), 13(a)–13(c) and 14(a)–14(c) also depict that the power efficiency of prototype SBVCVT is lower than 80% for the SBVCVT which is lower than 90% as reported in [51]. It is believed that some factors in the tests such as sensor noise, vibration, and component misalignment due to manufacturing error are the causes of lower transmission efficiency, but it is not the only reason. Since the excessive secondary clamping forces for the prototype DBVCVT were applied to the analytical model of the DBVCVT, it is believed that the excessive secondary clamping forces increase the wear of prototype DBVCVT and lower the power transmission efficiency. Figures 12–14 illustrate that the simulation results are in agreement with the experimental results, so it can be concluded that the low transmission efficiency of the prototype DBVCVT is mainly caused by the excessive secondary clamping forces. In fact, the excessive secondary clamping forces in Table 2 can prevent the belt from the slippage at utmost. The strategy of excessive

Table 4: Mean transmission efficiency of experimental results of DBVCVT.

| Speed ratio increases | | | Speed ratio decreases | | |
|---|---|---|---|---|---|
| Input speed $n_i$ (RPM) | Input torque $T_{i,2}$ (N·m) | Mean transmission efficiency $\eta_{\text{mean}}$ (%) | Input speed $n_i$ (RPM) | Input torque $T_{i,2}$ (N·m) | Mean transmission efficiency $\eta_{\text{mean}}$ (%) |
| 500 | 24.3 | 54.53 | 500 | 24.3 | 58.81 |
| | 54.3 | 62.48 | | 54.3 | 65.05 |
| | 78.8 | 58.85 | | 78.8 | 61.54 |
| | 107.6 | 61.82 | | 107.6 | 61.58 |
| 800 | 24.3 | 53.79 | 800 | 24.3 | 57.11 |
| | 54.3 | 60.83 | | 54.3 | 62.79 |
| | 78.8 | 58.23 | | 78.8 | 60.46 |
| | 107.6 | 62.19 | | 107.6 | 63.13 |
| 1200 | 24.3 | 53.85 | 1200 | 24.3 | 56.26 |
| | 54.3 | 58.42 | | 54.3 | 59.58 |
| | 78.8 | 56.33 | | 78.8 | 60.70 |
| | 107.6 | 60.37 | | 107.6 | 61.68 |

clamping force is commonly adopted by many existing automotive CVTs [51]. Besides, Figures 12(a)–12(c), 13(a)–13(c) and 14(a)–14(c) show the mean power efficiency of SBVCVT is approximately 10% higher than that of DBVCVT. It can be explained from the perspective of conservation of energy that more components in the DBVCVT definitely lead to high internal friction loss. However, this 10% low efficiency is only applicable for low driving torque. When the driving torque is over 88 N·m in the test, SBVCVT cannot transmit power, so Figures 12(d), 13(d), and 14(d) only show the experimental and simulation results of transmission efficiency of DBVCVT under $T_{i,2}$ = 107.6 N·m and different input speeds. Table 4 also shows the mean transmission efficiency of the DBVCVT under this condition. It can be concluded that, for the input torque over 88 N·m, the proposed DBVCVT as shown in Figures 12(d), 13(d), and 14(d) and Table 4 can still run stably and keep the maximum transmission efficiency over 70%. In other words, the proposed DBVCVT can improve the torque capacity as compared to SBVCVT and has a potential for heavy-duty vehicle transmissions.

(2) Figures 12–14 and Table 4 show the comparison of experimental results of the transmission efficiency under different input torques. It can be depicted that, under the same input torque, the transmission efficiency under $n_i$ = 500 RPM as shown in Figure 12 is universally higher than the transmission efficiency under $n_i$ = 800 RPM or $n_i$ = 1200 RPM as shown in Figures 13 and 14. It is because as the input speed is increased, the combined action of the tensile force of the steel ring and the extrusion force of the steel element is accordingly increased, improving the power transmission. But, the impact of input speed on the transmission efficiency is considered as limited because the curves of transmission efficiencies under $n_i$ = 800 RPM and $n_i$ = 1200 RPM are substantially coincident in Figures 13 and 14.

(3) Figures 12–14 and Table 4 also show the comparison of experimental results of the transmission efficiencies under different input speeds. From the above analysis of speed ratio test, it can be concluded that the hysteresis of the primary clamping force can cause different speed ratio responses when the speed ratio increases or decreases. From Table 4, the mean transmission efficiency of experimental results of the DBVCVT when the speed ratio increases is slightly lower than the mean transmission efficiency of experimental results of the DBVCVT when the speed ratio decreases. In fact, when the speed ratio decreases, the higher clamping force is more inclined to play its full role of transmitting the power than the relative lower one when the speed ratio increases.

(4) From the curves in Figures 12–14, it can be seen that under the same input torque and input speed, the overall transmission efficiency under $i < 1$ is lower than that under $i \geq 1$. As the speed ratio decreases, the transmission efficiency drops significantly. It is because the torque is transmitted by the combined action of tensile force of the steel ring and extrusion force of the steel element. Under $i < 1$, the combined action of forces hampers the torque transmission, resulting in more power losses under the same input power when the belt is moving inward or outward the pulleys. Under $i \geq 1$, the combined action of forces promotes the torque transmission, resulting in less power losses under the same input power when the belt is moving inward or outward the pulleys. In all, this is related to different dynamics of the DBVCVT when transmitting the torque under high transmission ratios ($i < 1$) and low transmission ratios ($i \geq 1$).

In this work, the authors design and implement some basic performance tests based on the proposed test rig. By comparing the experimental results with the simulation results based on the developed analytical model, some characteristics of the DBVCVT in the analytical model are validated by these basic performance tests. The feasibility of the test rig and the correctness of the analytical model can be coupled to lay the foundation for controlling the DBVCVT in order to achieve the accurate speed ratio, low slip, and high transmission efficiency.

## 4. Conclusions

Up to now, there is little research on the development of the test rig for DBVCVT. In order to prove the working principle of DBVCVT and analyze its transmission performance, this paper originally builds a light-load hardware-in-the-loop

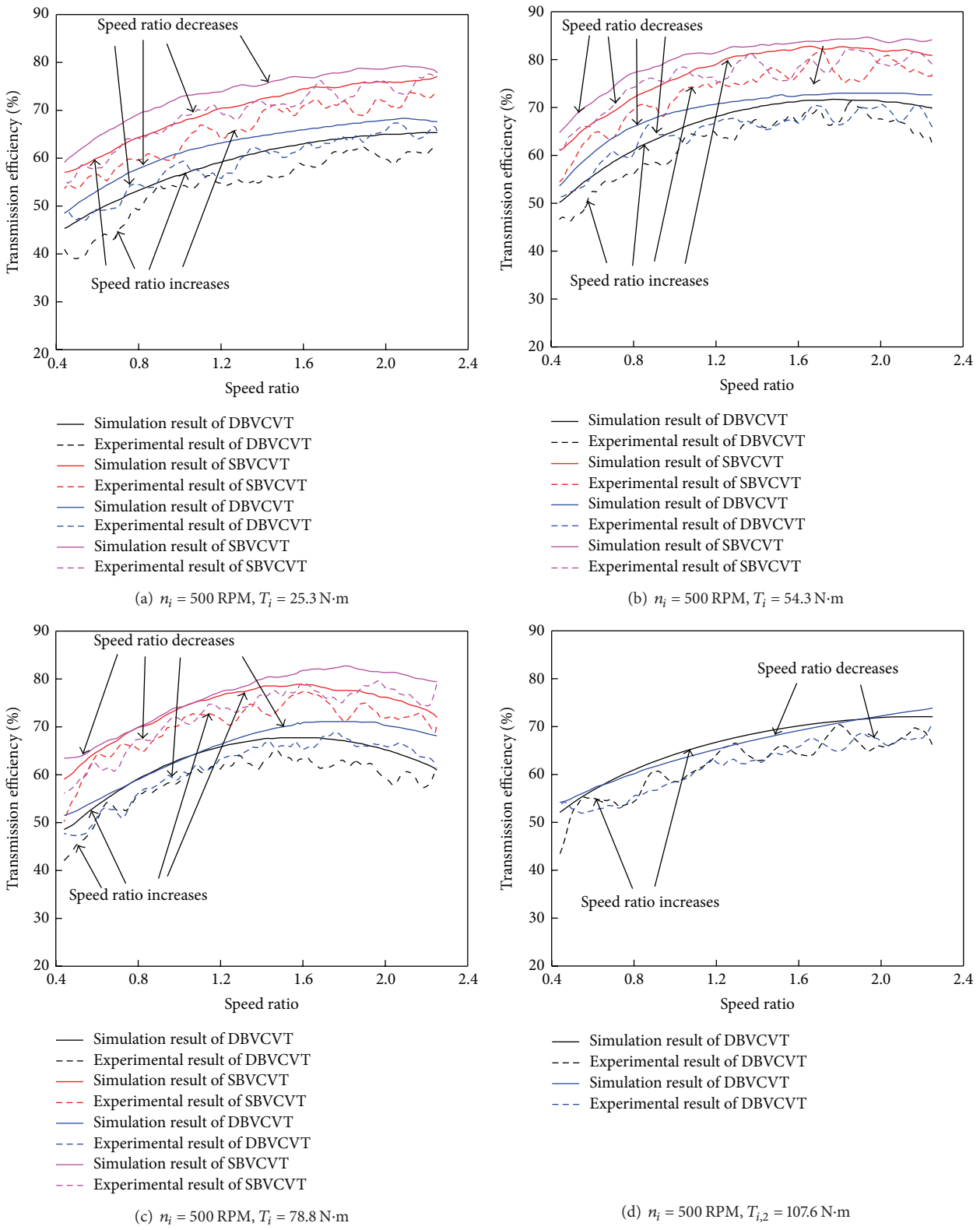


(a) $n_i$ = 500 RPM, $T_i$ = 25.3 N·m

(b) $n_i$ = 500 RPM, $T_i$ = 54.3 N·m

(c) $n_i$ = 500 RPM, $T_i$ = 78.8 N·m

(d) $n_i$ = 500 RPM, $T_{i,2}$ = 107.6 N·m

Figure 12: Comparison of simulation and experimental results of transmission efficiencies under $n_i$ = 500 RPM.

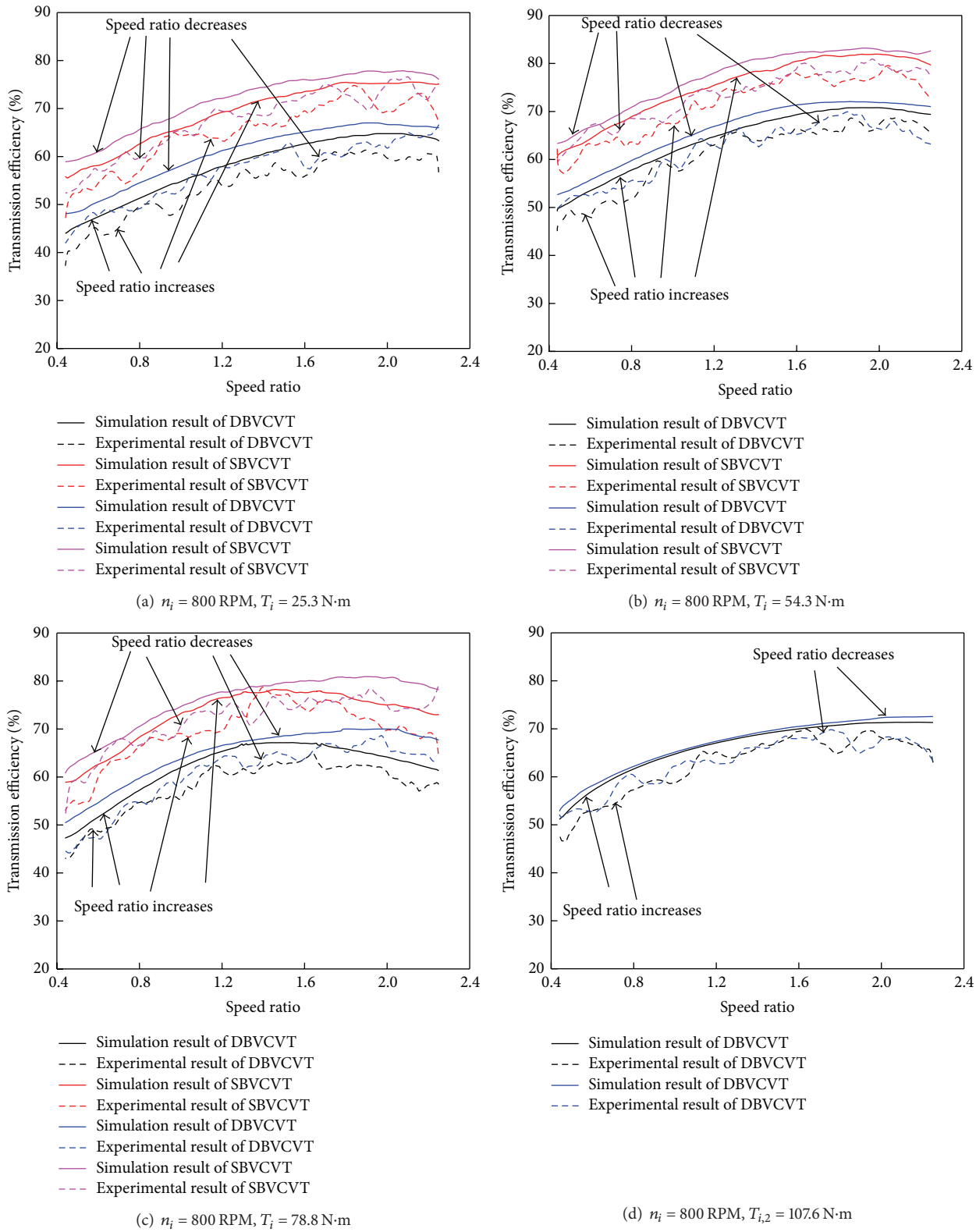


Figure 13: Comparison of simulation and experimental results of transmission efficiencies under $n_i$ = 800 RPM.

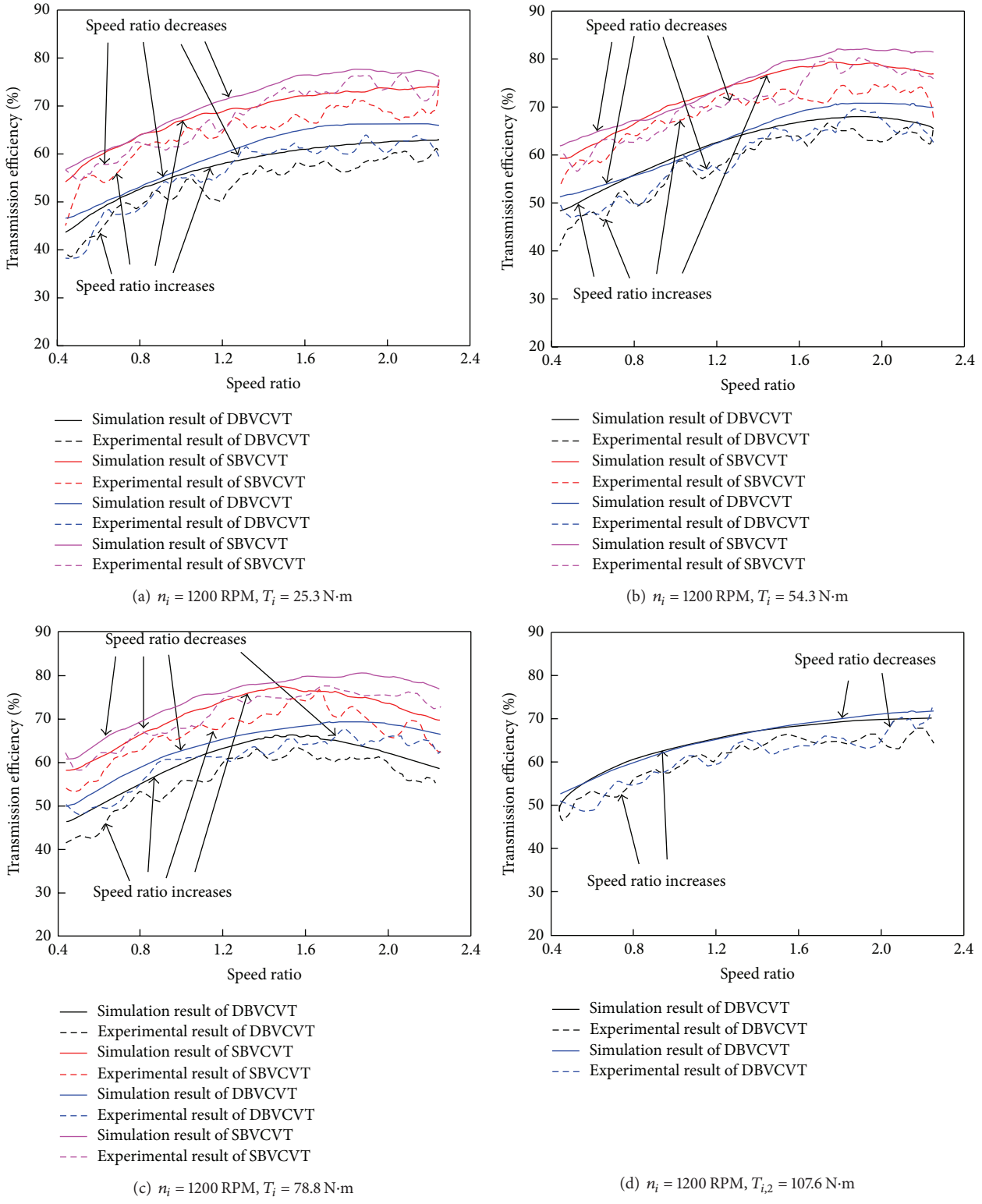


Figure 14: Comparison of simulation and experimental results of transmission efficiencies under $n_i$ = 1200 RPM.

test rig with a newly fabricated prototype of DBVCVT. By replacing the engine and load equipment with the AC motor and magnetic powder dynamometer, this test rig of DBVCVT aims to run under light-load conditions with simpler structure and lower cost and power consumption than the tradition test rig for SBVCVT. With this newly built test rig, the experimental investigation of DBVCVT is then implemented in this work and some conclusions can be drawn as follows:

(1) The test rig of DBVCVT is very durable and reliable in experimental studies.

(2) In the speed ratio test, the good agreement between experimental results and simulation results under different test conditions validates the relationship between the primary clamping force and the speed ratio change, specifying that the hysteresis of the primary clamping force always exists in the DBVCVT when shifting. The working principle actually is in accordance with the analytical model which was previously proposed by the authors. Therefore, this analytical model has been experimentally validated and can be used for simulation studies of DBVCVT.

(3) In the transmission efficiency test, some impacts on the transmission efficiency are analyzed by the comparison between the experimental and simulation results from the validated analytical model. Although the transmission efficiency under a lower input speed is slightly higher than the transmission efficiency under a higher input speed, the impact of input speed on the transmission efficiency is very little. Moreover, the hysteresis of the primary clamping force which can cause the mean transmission efficiency when the speed ratio increases is lower than the one when the speed ratio decreases. Besides, the overall transmission efficiency under $i < 1$ is lower than that under $i \geq 1$ due to different dynamics of the DBVCVT under different speed ratios when transmitting the power.

The above promising results show that the newly developed test rig of DBVCVT can provide a good platform for analyzing the transmission performance of DBVCVT. More complicated tests can be done since the working principle has been proved. Coupled with the analytical model, this test rig can be used to lay analytical and experimental foundations for further controlling the novel DBVCVT in order to achieve the accurate speed ratio, low belt slip, and high transmission efficiency.

## Nomenclature

$a$: Center-to-center distance
$B$: Distance between centerline of steel belt and centerline of inverse differential gearbox
$C$: Axial misalignment of belt
$C_e$: Mass of steel element per unit length
$C_r$: Mass of steel ring per unit length
$d_b$: Bearing mean diameter
$d_w$: Mean diameter of screw thread
$F_A = F_p(0) = F_s(0)$: Tensile force at the exit of primary pulley or tensile force at the entry of secondary pulley
$f_b$: Bearing torque loss factor
$F_B = F_p(\beta_p) = F_s(\beta_s)$: Tensile force at the entry of primary pulley or tensile force at the exit of secondary pulley
$F_p = F_p(\beta)$: Distribution of tensile force of steel ring on primary pulley
$F_{\text{pre}}$: Preload spring force
$F_{rp} = F_{rp}(\beta)$: Distribution of radial friction between steel element and primary pulley
$F_{rs} = F_{rs}(\beta)$: Distribution of radial friction between steel element and secondary pulley
$F_s = F_s(\beta)$: Distribution of tensile force of steel ring on secondary pulley
$h$: Radial distance from contact surface between steel ring and steel element to center of gravity of steel element
$h_e$: Thickness of each steel element
$h_r$: Thickness of each layer in steel ring
$i$: Transmission ratio
$i_g$: Geometric ratio
$i_{g,0}$: Speed ratio under no load when there is no axial misalignment of belt
$i_{\max}$: Maximum transmission ratio
$i_{\min}$: Minimum transmission ratio
$i_w$: Speed ratio of gearbox
$K$: Experimental constant of effective radius
$K_{\text{spring}}$: Spring stiffness
$K_t$: Torque distribution coefficient of inverse differential gearbox
$L$: Working length of steel belt
$m_e$: Mass of each steel element
$n$: Number of metal belts
$n_i$: Input speed
$n_{mp}$: Angular speed of primary DC servo motor
$n_{ms}$: Angular speed of secondary DC servo motor
$n_o$: Output speed
$n_{o1}$: Output speed of secondary pulley 1
$n_{o2}$: Output speed of secondary pulley 2
$N_r$: Number of layers in steel ring
$P_1$: Power loss due to radial friction between steel element and pulley
$P_2$: Power loss due to tangential friction between steel element and pulley
$P_3$: Power loss due to friction between inner layer of steel ring and contact surface of steel element

$P_4$: Kinetic energy loss of steel element
$P_5$: Power loss due to speed-dependent bearing frictional torque of input shaft
$P_6$: Power loss due to speed-dependent bearing frictional torque of output shaft
$Q_{p,n}$: Total axial clamping force of primary pulley for $n$-belt VCVT system
$Q_{ps} = Q_{ps}(\beta)$: Distribution of axial clamping force of primary pulley of one individual SBVCVT
$Q_{s,n}$: Total axial clamping force of secondary pulley for $n$-belt VCVT system
$Q_{ss} = Q_{ss}(\beta)$: Distribution of axial clamping force of secondary pulley of one individual SBVCVT
$r_0$: Working radius of pulley without axial misalignment under $i_{g,0} = 1$
$r_p$: Working radius of primary pulley
$r_{pi}$: Effective radius at the entry of primary pulley
$r_{po}$: Effective radius at the exit of primary pulley
$r_s$: Working radius of secondary pulley
$r_{si}$: Effective radius at the entry of secondary pulley
$r_{so}$: Effective radius at the exit of secondary pulley
$S_w$: Pitch of screw thread
$T_{i,n}$: Input torque for $n$-belt VCVT system
$T_{mp}$: Driving torque of primary DC servo motor
$T_{ms}$: Driving torque of secondary DC servo motor
$v_b$: Kinematic viscosity of lubricant
$V_e$: Tangential velocity of steel element based on effective radius
$v_p$: Tangential velocity of primary pulley
$v_s$: Tangential velocity of secondary pulley
$\alpha$: Angle between the vertical centerline of shaft and the tangent point of steel belt
$\beta_p$: Angle of wrap of a belt on primary pulley
$\beta_s$: Angle of wrap of a belt on secondary pulley
$\gamma$: Sliding angle
$\Delta n$: Speed difference between $n_{o1}$ and $n_{o2}$
$\Delta r_p$: Axial moving displacement of primary pulley
$\Delta r_s$: Axial moving displacement of secondary pulley
$\varepsilon$: Slip ratio
$\eta_d$: Efficiency of gear train in inverse differential gearbox
$\eta_{dt}$: Transmission efficiency of inverse differential gearbox
$\eta_{\text{mean}}$: Mean of actual transmission efficiency
$\eta_n$: Power transmission efficiency
$\theta_{mp}$: Rotational degree of primary DC servo motor
$\theta_{ms}$: Rotational degree of secondary DC servo motor
$\theta_p$: Groove angle of primary pulley
$\theta_s$: Groove angle of secondary pulley
$\lambda_w$: Lead angle of screw thread
$\mu_{\text{ep}}$: Friction coefficient between steel element and pulley
$\mu_{\text{re}}$: Friction coefficient between steel ring and steel element
$\rho_w$: Equivalent friction angle
$\omega_p$: Angular velocity of primary pulley
$\omega_s$: Angular velocity of secondary pulley.

## Conflict of Interests

The authors declare that there is no conflict of interests regarding the publication of this paper.

## Acknowledgment

The project is supported by the University of Macau Research Grants nos, MYRG2014-000058-FST and MYRG077(Y1-L2)-FST13-WPK.

## References

[1] H. Dong, Y. Cao, and Z. Fang, "Dynamic vibration characteristic analysis for the power-split transmission system based on loaded tooth contact analysis," *Shock and Vibration*. In press.

[2] G. Mantriota, "Fuel consumption of a vehicle with power split CVT system," *International Journal of Vehicle Design*, vol. 37, no. 4, pp. 327–342, 2005.

[3] T. Toyoda, T. Imanishi, and E. Inoue, "Fuel economy improvement items with toroidal continuously variable transmission," in *Proceedings of the CVT-Hybrid International Conference*, pp. 67–72, 2010.

[4] F. Bottiglione, G. Carbone, L. D. Novellis, L. Mangialardi, and G. Mantriota, "Mechanical hybrid KERS based on toroidal traction drives: an example of smart tribological design to improve terrestrial vehicle performance," *Advances in Tribology*, vol. 2013, Article ID 918387, 9 pages, 2013.

[5] F. Bottiglione and G. Mantriota, "Effect of the ratio spread of CVU in automotive kinetic energy recovery systems," *Transactions of the ASME—Journal of Mechanical Design*, vol. 135, no. 6, Article ID 061001, 2013.

[6] G. Carbone, L. Mangialardi, and G. Mantriota, "Theoretical model of metal V-belt drives during rapid ratio changing," *Journal of Mechanical Design*, vol. 123, no. 1, pp. 111–117, 2001.

[7] G. Carbone, L. Mangialardi, and G. Mantriota, "Influence of clearance between plates in metal pushing V-belt dynamics," *Journal of Mechanical Design*, vol. 124, no. 3, pp. 543–557, 2002.

[8] G. Carbone, L. Mangialardi, and G. Mantriota, "The influence of pulley deformations on the shifting mechanism of metal belt CVT," *Journal of Mechanical Design*, vol. 127, no. 1, pp. 103–113, 2005.

[9] G. Carbone, L. Mangialardi, B. Bonsen, C. Tursi, and P. A. Veenhuizen, "CVT dynamics: theory and experiments," *Mechanism and Machine Theory*, vol. 42, no. 4, pp. 409–428, 2007.

[10] N. Srivastava and I. Haque, "A review on belt and chain continuously variable transmissions (CVT): dynamics and control," *Mechanism and Machine Theory*, vol. 44, no. 1, pp. 19–41, 2009.

[11] B. Bonsen, T. W. G. L. Klaassen, K. G. O. Van de Meerakker, M. Steinbuch, and P. A. Veenhulzen, "Analysis of slip in a continuously variable transmission," in *Proceedings of the ASME International Mechanical Engineering Congress (IMECE '03)*, pp. 995–1000, November 2003.

[12] H. Kim and J. Lee, "Analysis of belt behavior and slip characteristics for a metal V-belt CVT," *Mechanism and Machine Theory*, vol. 29, no. 6, pp. 865–876, 1994.

[13] W. Ryu and H. Kim, "CVT ratio control with consideration of CVT system loss," *International Journal of Automotive Technology*, vol. 9, no. 4, pp. 459–465, 2008.

[14] Nissan Maxima, 2013, http://www.nissanusa.com/maxima/specifications.html.

[15] F. Sorge, "Variational approach to the mechanics of metal V-belt systems," *International Journal of Vehicle Design*, vol. 39, no. 3, pp. 189–207, 2005.

[16] K. Narita and M. Priest, "Metal-metal friction characteristics and the transmission efficiency of a metal V-belt-type continuously variable transmission," *Proceedings of the Institution of Mechanical Engineers Part J: Journal of Engineering Tribology*, vol. 221, no. 1, pp. 11–26, 2007.

[17] N. Srivastava and I. Haque, "On the transient dynamics of a metal pushing V-belt CVT at high speeds," *International Journal of Vehicle Design*, vol. 37, no. 1, pp. 46–66, 2005.

[18] N. Srivastava and I. Haque, "Transient dynamics of the metal V-belt CVT: effects of pulley flexibility and friction characteristics," *Journal of Computational and Nonlinear Dynamics*, vol. 2, no. 1, pp. 86–97, 2007.

[19] N. Srivastava and I. Haque, "Transient dynamics of metal V-belt CVT: effects of band pack slip and friction characteristic," *Mechanism and Machine Theory*, vol. 43, no. 4, pp. 459–479, 2008.

[20] C. H. Zheng, W. S. Lim, and S. W. Cha, "Performance optimization of CVT for two-wheeled vehicles," *International Journal of Automotive Technology*, vol. 12, no. 3, pp. 461–468, 2011.

[21] A. Karam and D. Play, "A discrete analysis of metal-v belt drive," in *Proceedings of the ASME International Power Transmission and Gearing Conference*, vol. 43, pp. 319–327, 2013.

[22] B. Supriyo, K. B. Tawi, and H. Jamaluddin, "Experimental study of an electro-mechanical CVT ratio controller," *International Journal of Automotive Technology*, vol. 14, no. 2, pp. 313–323, 2013.

[23] K. U. Chan, P. K. Wong, and H. W. Wu, "Preliminary study on design and control of a novel CVT," JSAE Paper 20097011, 2009.

[24] A. W. Brown, J. van Rooij, and A. A. Frank, "The design of an inline GCI chain cvt for large vehicles," in *Proceedings of the International Continuously Variable and Hybrid Transmission Congress*, no. 54, September 2004.

[25] M. F. Oudijk, *Optimization of CVT control for hybrid and conventional drive lines [M.S. thesis]*, Eindhoven University of Technology, 2005.

[26] H. Sattler, "Efficiency of metal chain and V-belt CVT," in *Proceedings of the International Congress on Continuously Variable Power Transmission (CVT '99)*, Eindhoven, The Netherlands, September 1999.

[27] Luk, 2012, http://www.luk.de/content.luk.de/en/.

[28] Transmissions, 2013, http://automotive.roger.free.fr/main_pages/main_transmission.html.

[29] Y. Q. Chen, P. K. Wong, Z. C. Xie, H. W. Wu, K. U. Chan, and J. L. Huang, "Modelling of a novel dual-belt continuously variable transmission for automobiles," *World Academy of Science, Engineering and Technology*, no. 70, pp. 1157–1161, 2012.

[30] K. Hagiwara, S. Terayama, Y. Takeda, K. Yoda, and S. Suzuki, "The development and utilization of hardware-in-the-loop simulation for the development of an automatic transmission control system," SAE Paper No. 2002-01-1255, 2002.

[31] K. Hagiwara, S. Terayama, Y. Takeda, K. Yoda, and S. Suzuki, "Development of automatic transmission control system using hardware-in-the-loop simulation system," *JSAE Review*, vol. 23, no. 1, pp. 55–59, 2002.

[32] K. Hagiwara, R. Ito, K. Yoda, and H. Saotome, "Development of transient state model for CVT-HILS," *Honda R&D Technical Review*, vol. 17, no. 1, pp. 65–72, 2005.

[33] S. Bai, R. Moses, T. Schanz, and M. Gorman, "Development of a new clutch-to-clutch shift control technology," SAE Paper No. 2002-01-1252, 2002.

[34] T. Matsumura, S. Ichikawa, F. Katsu, and M. Sato, "The development of a controller confirmation system for automatic transmissions and its applications," in *Proceedings of the IEEE International Conference on Control Applications*, pp. 1415–1419, September 2004.

[35] T. Brendecke and F. Küçükay, "Virtual real-time environment for automatic-transmission control units in the form of hardware-in-the-loop," *International Journal of Vehicle Design*, vol. 28, no. 1, pp. 84–102, 2002.

[36] Q. Z. Yan, J. M. Williams, and J. Li, "Chassis control system development using simulation: software in the loop, rapid prototyping, and hardware in the loop," SAE Paper No. 2002-01-1565, 2002.

[37] Q. Z. Yan, F. C. Thompson, R. E. Paul, and J. J. Bielenda, "Hardware in the loop for dynamic chassis control algorithms test and validation," SAE Paper No. 2004-01-2059, 2004.

[38] Q. Z. Yan, F. Oueslati, J. Bielenda, and J. Hirshey, "Hardware in the loop for a dynamic driving system controller testing and validation," SAE Paper No. 2005-01-1667, 2005.

[39] W. H. Oh, J. H. Lee, H. G. Kwon, and H. J. Yoon, "Model-based development of automotive embedded systems: a case of continuously variable transmission (CVT)," in *Proceedings of the 11th IEEE International Conference on Embedded and Real-Time Computing Systems and Applications*, pp. 201–204, August 2005.

[40] J. Steiber, B. Surampudi, M. Rosati, M. Turbett, R. Hansen, and T. Tower, "Modeling, simulation, and hardware-in-the-loop transmission test system software development," SAE Paper No. 2003-01-0673, 2003.

[41] J. Steiber, B. Surampudi, B. Treichel, and M. Kluger, "Vehicle HIL, the near term solution for optimizing engine and transmission development," SAE Paper No. 2005-01-1050, 2005.

[42] *An Automated Design Synthesis System Involving Hardware-In-the-Loop Simulation*, 2014, http://www.opal-rt.com/fr/node/383.

[43] X.-A. Sun, G.-Q. Wu, L. He, and G.-L. Kong, "Hardware-in-the-loop simulation for electro-control system of continuously variable transmission based on dSPACE," in *Proceedings of the IEEE Vehicle Power and Propulsion Conference (VPPC '08)*, pp. 1–5, September 2008.

[44] S. W. Yang and D. Q. Zhao, "Object-oriented modeling and real-time simulation of planetary gearbox with modelica and simulink," in *Proceedings of the 6th International Symposium on Test and Measurement*, pp. 773–776, 2005.

[45] M. R. Turbett, R. M. Senseney, S. D. Nash et al., "Virtual vehicle transmission test cell," Google Patents, 2004.

[46] S. Gao, Y. An, Y.-S. Zhou, and C.-X. Song, "CVT fault diagnosis based on immune principle and oil spectrum analysis," in *Proceedings of the IEEE 5th International Conference on Bio-Inspired Computing: Theories and Applications (BIC-TA '10)*, pp. 1106–1110, IEEE, Changsha, China, September 2010.

[47] F. Katsu and T. Matsumura, "Practical use of HILS and an approach to MBCSD for AT and CVT development," in *Proceedings of the IEEE International Conference on Control Applications (CCA '06)*, pp. 2111–2114, Munich, Germany, October 2006.

[48] Q. Zheng, W. W. Chung, K. Defore, and A. Herman, "A hardware-in-the-loop test bench for production transmission controls software quality validation," SAE Paper 2007-01-0502, 2007.

[49] Q. Zheng, A. Habeebullah, W. W. Chung, and A. Herman, "A 6-speed automatic transmission plant dynamics model for HIL test bench," SAE Paper No. 2008-01-0630, 2008.

[50] Subaru, 2010, http://drive2.subaru.com/Sum09/Sum09_what-makes.htm.

[51] B. Bonsen, *Efficiency optimization of the push-belt CVT by variator slip control [Ph.D. thesis]*, Eindhoven University of Technology, Eindhoven, The Netherlands, 2006.

[52] H. A. Rothbart and T. H. Brown, *Mechanical Design Handbook*, McGraw-Hill, New York, NY, USA, 2006.

[53] J. Yamaguchi, K. Okubo, T. Fujii, R. Kido, and M. Takahasi, "Study on power transmitting efficiency of CVT using a dry hybrid V-belt," in *Proceedings of the 8th International Conference on Urban Transport and the Environment in the 21st Century*, pp. 807–816, 2002.

[54] J. L. Xu, X. Y. Su, and B. Peng, "Numerical analysis and demonstration: transmission shaft influence on meshing vibration in driving and driven gears," *Shock and Vibration*. In press.

[55] W. X. Liu, *Vehicle Axle Design*, Tsinghua University Press, 2004, (Chinese).